Technical University of Crete
School of Mineral Resources Engineering
Petroleum Engineering M.Sc. Course

History matching of production data using an updated static model. A case study from Gullfaks

Master Thesis by

Pyliotis Ioannis

thesis Examination Committee: Kalogerakis Nikolaos (Supervisor)
Chatzichristos Christos
Kiomourtzi Paschalia

Abstract

In the present thesis, a new dynamic model of H1 segment in the Gullfaks field, Norway, is built based on an updated static model. The update of the static model refers to the re-interpretation of a more recent seismic dataset, which resulted into a new structural model. The new static model was the basis for constructing a new grid for dynamic modelling for history matching.

Two different datasets were combined for this purpose. The first dataset was an already existing dynamic model for H1 segment (Lower Brent Group) and production data, while the second one was a 3D seismic dataset along with a static model of the overlying Upper Brent Group for the entire Gullfaks field (Petrel support dataset).

The predictions of the new dynamic model were different compared to those of the initial dynamic model, which most probably reflects the impact of the updated structure. However, based on the interpretation of the available seismic data it is considered that the updated structure is more consistent to geological setting of the area that the seismic reveal. Thus, by having a more representative geological static model and the production data history matched on the new grid, we can conclude that the updated dynamic model can predict the future performance of the studied reservoir with more confidence.

Table of Contents

1 Introduction

1.1 Motivation

In the oil industry, the use of 3D modelling techniques in reservoir modelling have been proved extremely useful because it is a handy way to represent the structure of a field, to assess H/C volumes in place, propose new wells, to plan the production, to predict the behavior of the reservoir under production, etc. Models, generally, are distinguished into static and dynamic. Usually the geologist and the geophysicists are responsible of the static model construction, while dynamic models constitute a specialty of the engineers, without excluding the collaboration of the two teams.

Models' update in the presence of new data is a must and it is an ongoing procedure throughout the life cycle of the reservoir depletion. This procedure requires the collaboration of a variety of different disciplines, dependent on the type of the new data, substantial amount of money spent by oil companies for the construction of reservoir models capable to predict with accuracy the response of the reservoir in future.

Such a model update of the H1 segment of the Lower Brent Group in Gullfaks oil field is presented in this study. The update is based mostly on a re-interpreted structure as it was observed on a more recent 3D seismic dataset. Property propagation throughout the new grid and history matching of the already existing production data give a new insight of the prediction of reservoir performance.

1.2 Objectives

- Re-interpretation of faults and Top- and Base-structure of Lower Brent Group based on a new seismic dataset
- Update an existing dynamic model with a different set of seismic data
- New static model construction
- Different alternative ways in structural frameworks and property propagation algorithms to capture the geological uncertainty
- Scale up properties (permeability, porosity, net-to-gross)

- Update the dynamic model based on the new static model
- Compare the efficiency of the different structural frameworks and property propagations
- Compare the efficiency of different dynamic models
- History match a new dynamic model by modifying transmissibilities

1.3 Thesis Outlines

This thesis' structure consists by 4 chapters and 2 appendices. The organization of the thesis is briefly described below:

- **Chapter 1** comprises an introduction for this work and consist of the motivation, the objectives and the organization of the thesis
- **Chapter 2** includes a brief introduction to the study area.
- **Chapter 3** starts with the presentation and evaluation of the available data. Afterwards the steps for constructing a series of updated statics and dynamic models are described. The evaluation of these dynamic models based on their prediction efficiency follows and after determining the model giving the best prediction, the procedure of matching the predictions of the model to the historical production data is described.

Finally, **Chapter 4** discusses the conclusions of the present thesis

2 Study area

The present thesis focus on H1 reservoir segment of the Gullfaks field. The main Gullfaks field is located in block 34/10 in the northern part of the Norwegian North Sea and discovered during 1978. StatoilHydro (70% ownership-operator) and Petoro (30% ownership) operate this field (statoil.com, Talukdar and Instefjord 2008).

The field has been developed with three concrete platforms; Gullfaks A, Gullfaks B and Gullfaks C (production began at 22/12/1986, 29/02/1988 and 4/11/1989 respectively) (statoil.com). The transport of the produced oil is exported from Gullfaks A and Gullfaks C via loading buoys onto tankers (Alveberg and Melberg 2013).

The recovery factor of the field is 59% but the goal is to increase into 62 % (statoil). The drive mechanisms are water injection, gas injection and water/alternating gas injection (WAG) (Alveberg and Melberg 2013).

Structurally Gullfaks field is subdivided into three parts. At the eastern part exist an eroded horst complex, at the west a domino fault system while between them there is an accommodation zone. The main faults of the domino area have a N-S strike dipping to the east with angles of about 30 degrees. Same strike faults are present to the horst complex but with a westward dipping angles of 60 to 65 degrees (Fossen and Hesthammer 1998, Rouby et al. 1996). The main fault blocks are subdivided into a number of smaller fault segments by a numerous of small-scale, east-west trending normal faults (over 300 are identified on the main field) (Talukdar and Instefjord 2008). In some cases, there is fluid and pressure communication between these segments while in other the faults act like barriers isolating those segments (Figure 2).

The stratigraphic sequence of Gullfaks field (Figure 3) includes (Hesthammer, and Fossen 2001):

- At the bottom, continental sediments of the Triassic Herge Group (interbedded sandstones, claystones and shales)
- Alluvial sandstones of the Rhaetian-Sinemurian Statfjord Formation
- Overlaid by Dunlin Group; Sinemurian-Toarcian marine clay- and

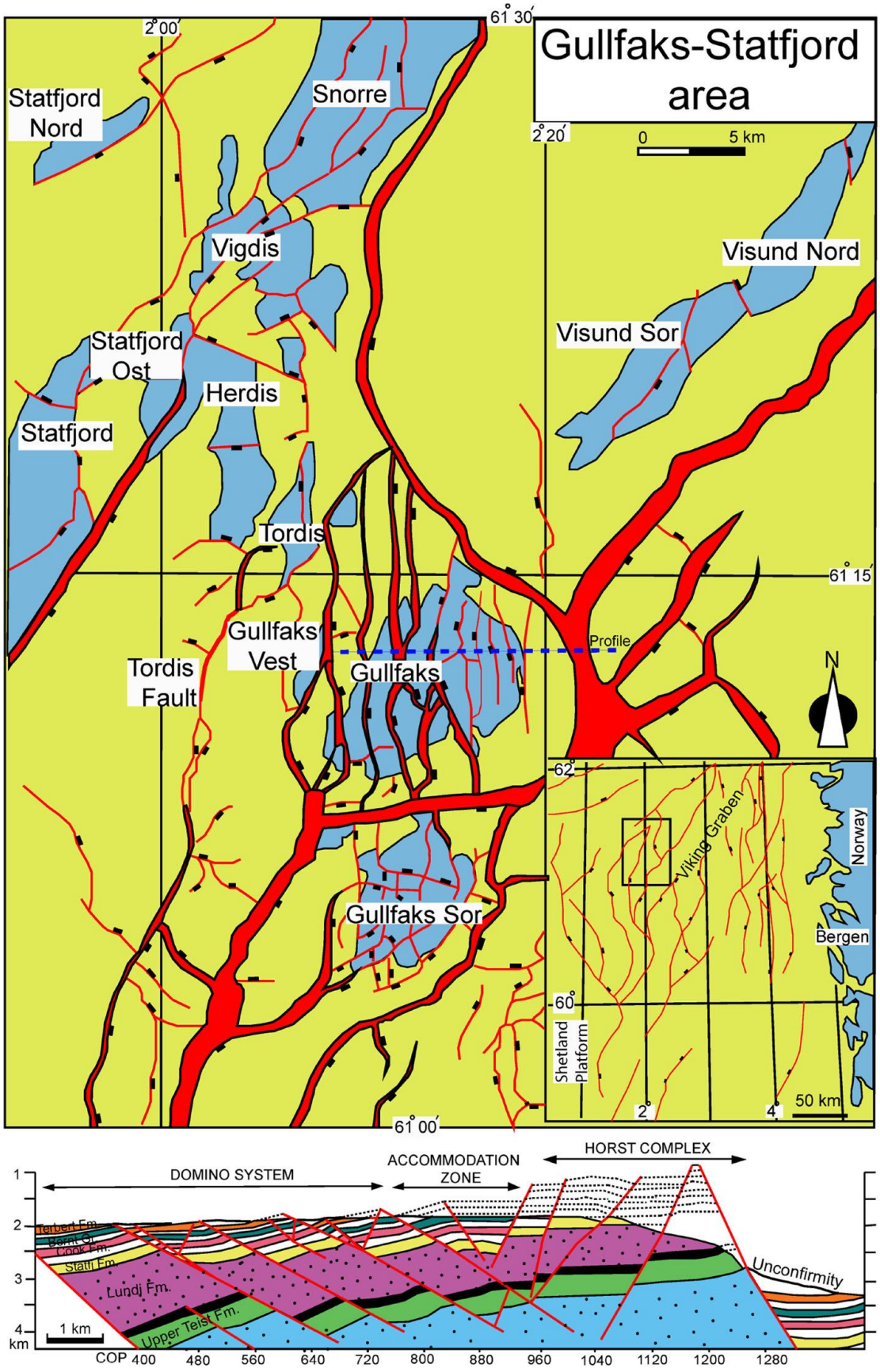

Figure 1 -Structural map and cross section of the Gullfaks field (from: Yielding et al. 1999 in Siddiqui et al. 2016)

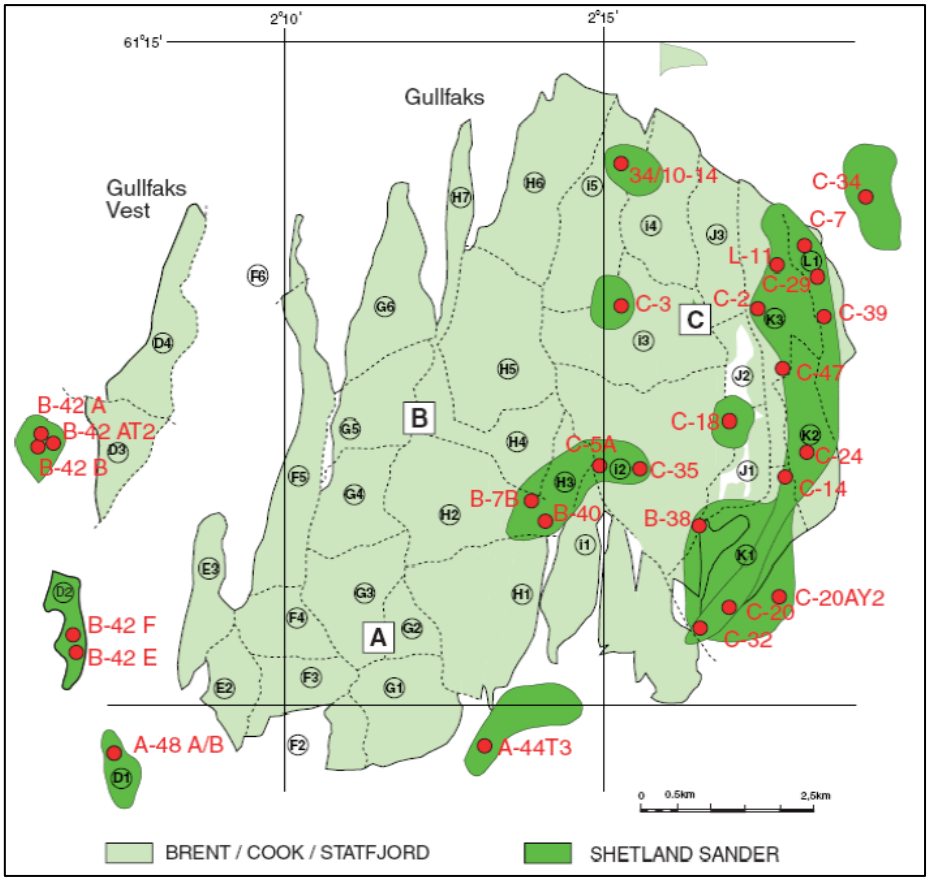

Figure 2 - Fluid segments on the Gullfaks Main Field (Gullfaks RMP 2007)

silt-stones of the Amundsen Formation, regressive, marine, silty claystones, muddy sandstones and sand of the Cook Formation, and marine shales and siltstones of the Drake Formation

- The uppermost part of the reservoir contains the deltaic sediment of the Bajocian-Early Bathonian Brent Group (Hesthammer and Fossen 2001, Rouby et al. 1996).

The Brent Group is subdivided into lower and upper:

- Lower Brent
  - Broom Formation(8-12m)
  - Rannoch Formation (50-90m)
  - Etive Formation (15-40m)
- Upper Brent
  - Ness (85-110m)
  - and Tarbert (75-105m)

The reservoir rocks in the Gullfaks area are capped by Cretaceous shales and siltstones. An unconformity, representing a time gap of up to 100My, defines the Cretaceous sediments (Hesthammer and Fossen 2001).

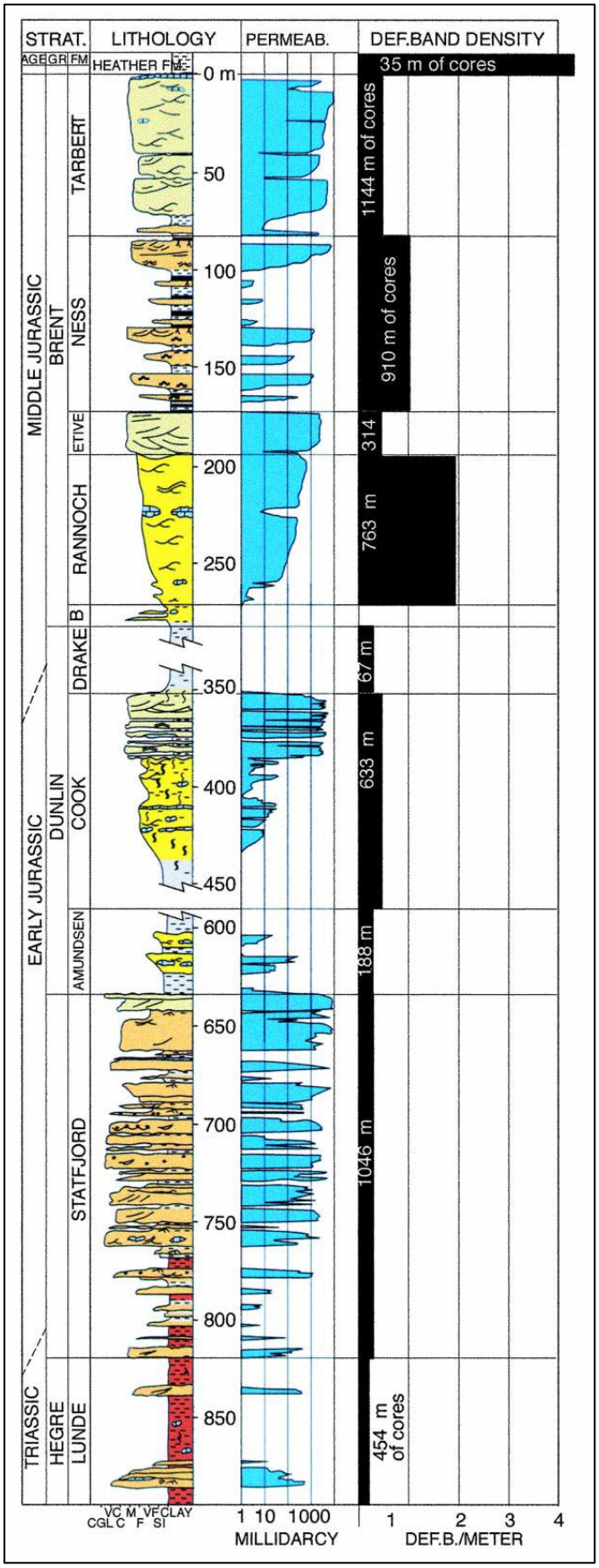

Figure 3 - Stratigraphic column for the Jurassic and Triassic reservoir units within the Gullfaks field. (Modified by Fossen (2001) after Tollfsen, Graue and Svinddal (1994))

3 Material and methods

3.1 Reservoir modeling

From the early starts of exploration till the late stages of exploitation of hydrocarbon reservoirs the use of 3D reservoir models is fundamental. These models are representations of the reservoir in a digitized form containing an enormous number of data relevant to the physical properties and the containing fluids of the reservoir.

There are two major types of 3d model; the static and the dynamic models. The first type is used to represent the static properties of a reservoir i.e. those that don't exhibit fluctuations over time, like reservoir geometry, permeability, porosity etc. On the other hand, dynamic models use static models as an input incorporating time-depended properties such as (relative permeability, fluid properties, well productivity etc.) and/or production data in order to simulate the behavior of the reservoir fluids as a function of production and/or injection by applying equations for fluid flow in porous media.

Reservoir modeling and simulation can be used for calculating STOIIP and recovery factors, for well planning, optimizing the depletion of the field, designing the appropriate facilities, estimating financial risks etc.

Reservoir modeling can utilize a wide variety of data sources. According Rivenæs et al 2010 such data sources are (Figure 4):

- Geophysical Data (mainly seismic data)
  - Interpreted horizons and faults, usually depth converted (Figure 4 a).
  - Seismic inversion data that provide important information on rock properties, e.g. porosity and fluid distribution.
  - 4D seismic data provide additional crucial information on reservoir behaviour during production, for instance connectivity and segmentation.
- Petrophysical Data
  - Porosity logs (Figure 4 f).
  - Microscopic images (thin sections and SEM) and laboratory analysis (XRD) for mineralogy and pore geometries taken from core samples (Figure 4 d).
  - Horizontal permeability

- Input on vertical permeability (often expressed as the Kv/Kh ratio between vertical and horizontal permeability
- Petrophysical lithology curves
- Input to fluid and saturation models – such as saturation logs, saturation height functions, fluid contacts, and fluid properties.

- Geological Data
  - Reservoir zonation and sedimentological description, including identification of flow units (modelling facies) and barriers.
  - Various stratigraphic models, including sequence stratigraphic models and lithostratigraphic models. This also includes palogeographic maps which may be quite important for understanding trends and architectural topology within reservoir units in the model construction.
  - Evaluation of compaction and diagenesis, including impact on reservoir property distribution.
- Reservoir Technical Data
  - Pressure data, both those observed prior to production and the pressure development during production.
  - Various fluid data and PVT data, such as viscosities, fluid densities, Bo, Bg (shrinkage factors for oil and gas), etc.
  - Well test data and production history in general. These data are usually applied during calibration of reservoir model, known as history matching.

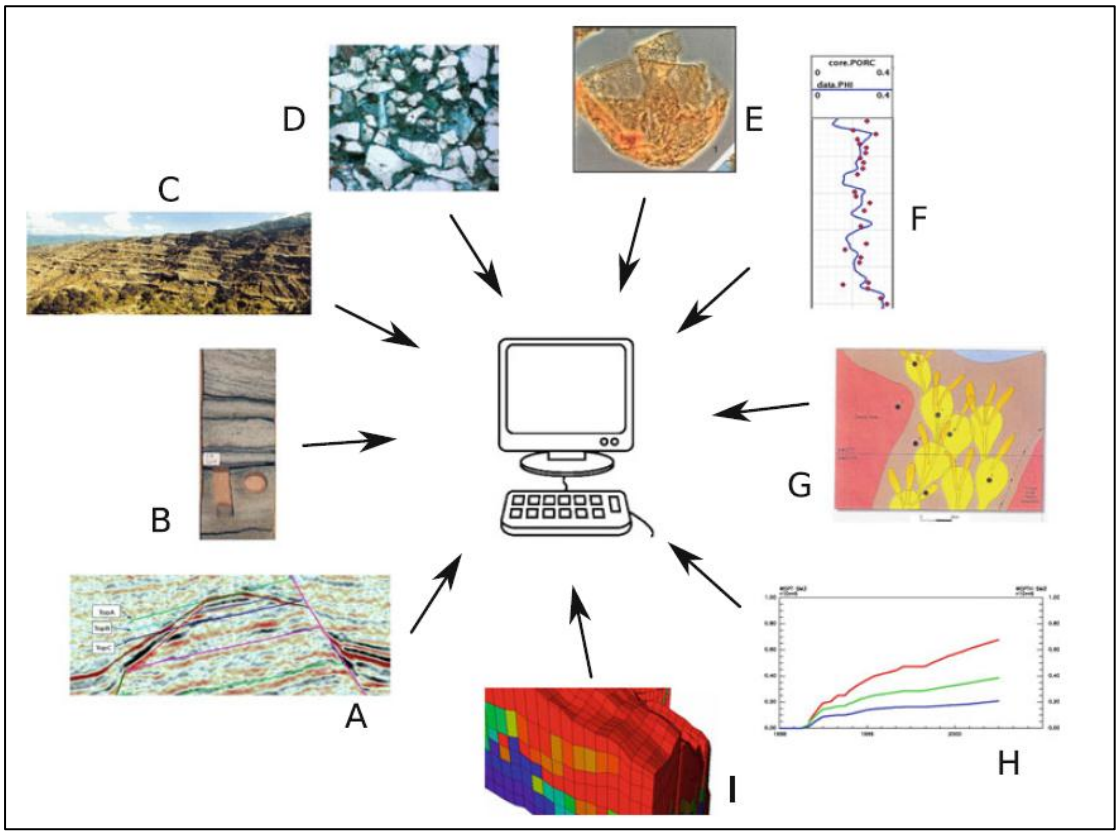

Figure 4 - Reservoir models integrate many data sources. These include seismic data (a), core data (b), outcrop analogues (c), thin sections (d), biostratigraphy (e), well logs and correlations (f), concept models (g), production data (h), and earlier reservoir models (i). These data originate from various subsurface disciplines at different scales, abundance and quality

- Databases and Data Management

  All data input to reservoir modelling need to be easily accessible. A database is an organized collection of data, and includes digital data as well as paper reports. The purpose of a database is to provide efficient retrieval for the task to be performed – in this case reservoir modelling.

3.2 Available data

For the needs of the present thesis two different datasets were used. The first one was a more recent 3D seismic cube along with a static model of the overlying Upper Brent Group with the following description:

- A Seismic cube

  which covers an area of 70 Km^2, containing 375 inlines with a total length 7.5Km and 301 crosslines with a total length of 9.332 Km
- Velocity model
- Interpreted horizons and fault

  The interpreted horizons included to the database describe the Upper Brent Group and they are, from the higher to the lower, Base Cretaceous, Top Tarbert, Tarbert 1, Tarbert 2, Top Ness, Ness 1 and Top Etive. These horizons are intersected by 16 faults (Figure 5, Figure 6).
- 15 wells

  along with their well headers (well location map), well deviations (well paths), well logs, and well tops (formation tops) (A10, A15, A16, B1, B2, B4, B8, B9, C1, C2, C3, C4, C5, C6, and C7).

The second dataset comprised by a dynamic model of the H1 segment of the Gullfaks field, in Eclipse format containing data for a twelve-year period between 1 December 1986 till 31 November 1998. As we already mentioned H1 segment belongs to Lower Brent. In more detail H1 dynamic model comprised by

- A reservoir grid
  with dimensions is 20 x 40 x 13; a total of 10400 grid cells from which 5144 are active (Figure 7a).
- 8 well paths;
  5 production wells (P-A1H, P-A2AH, P-A39A, P-A17 and P-A35) and 3 injectors (I-A38, I-A5H and I-H2) injectors (Figure 7b)
- Production/injection data for these wells
- PVT data

- Assigned rock properties to the grid cells (porosity, permeability, net-to-gross)

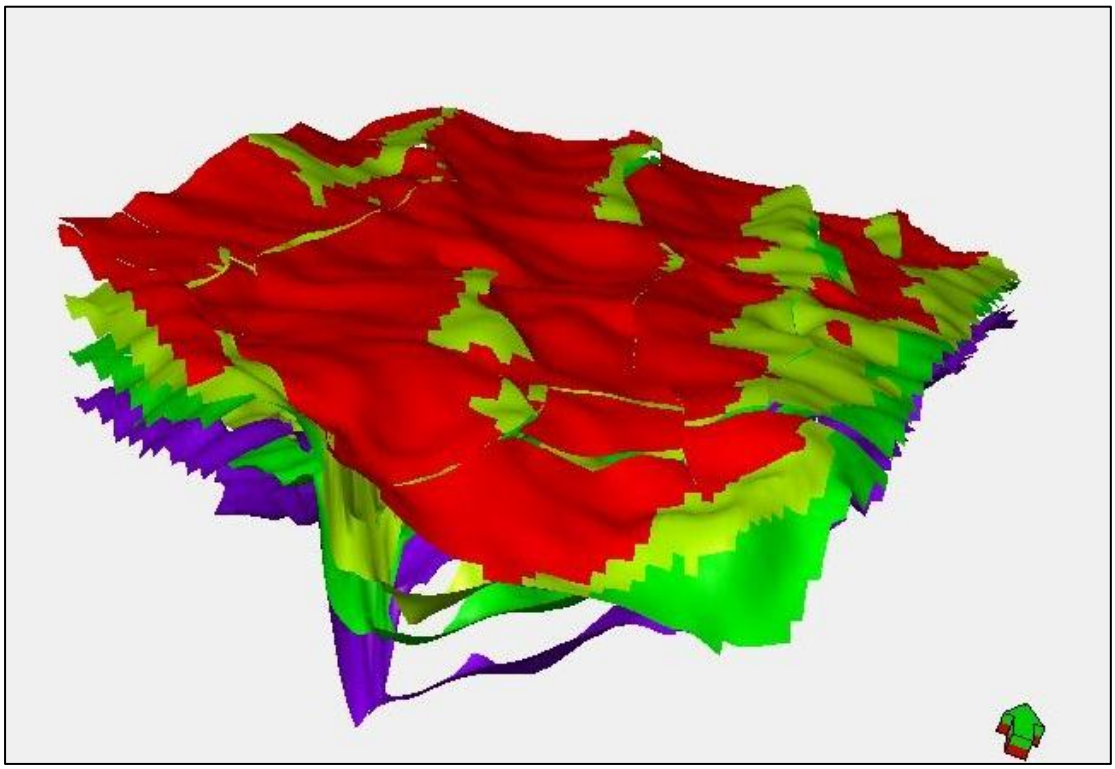

Figure 5 – Representation of the main four surfaces contained to Gullfaks dataset (Base Cretaceous-red, Top Tarbert-yellow, Top Ness-green and Top Etive-purple)

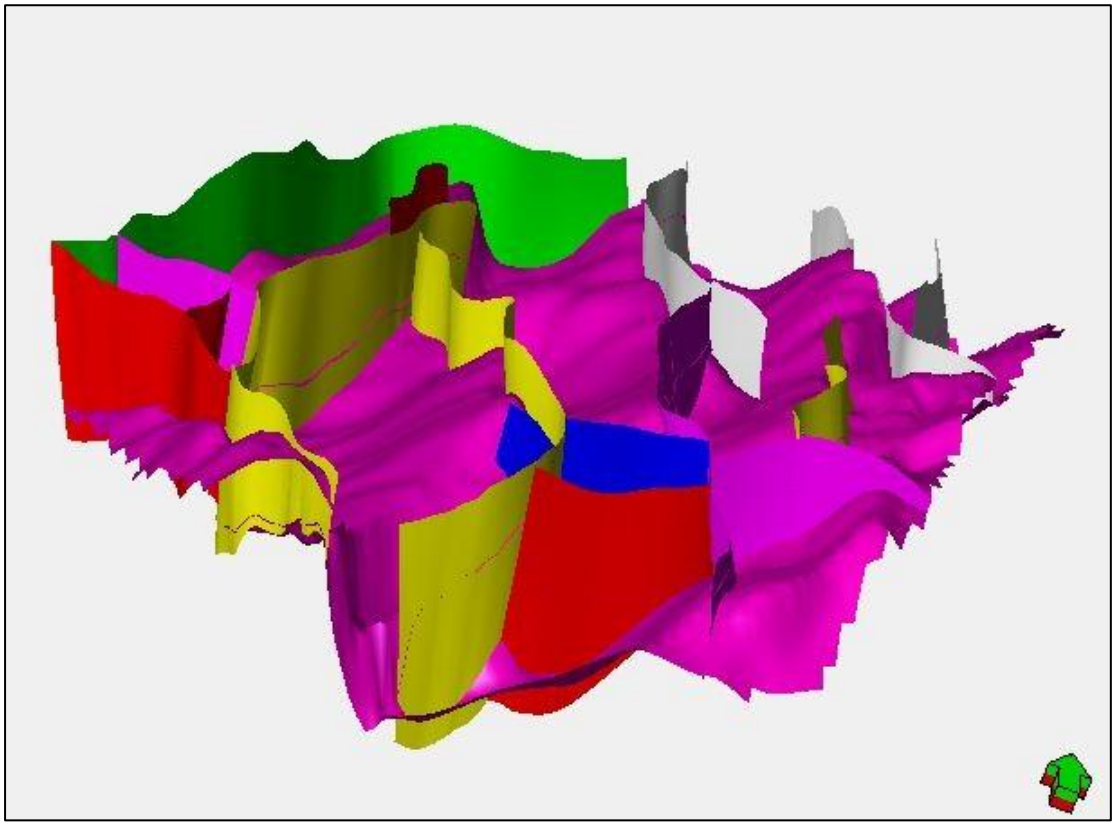

Figure 6 – Representation of the fault contained to the Gullfaks dataset. The purple surface corresponds to top Etive

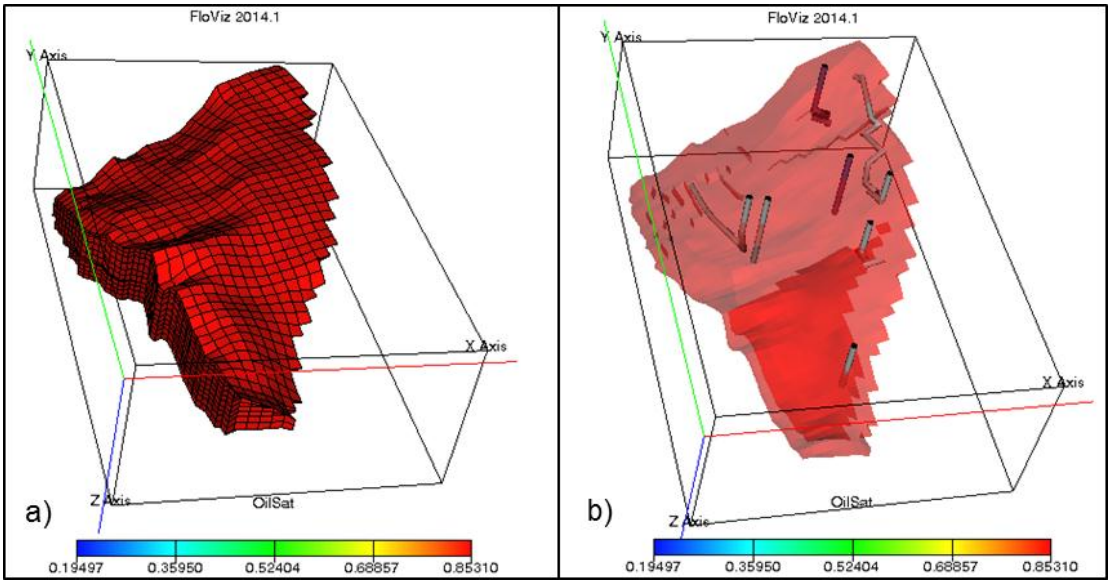

Figure 7 - a) The grid of the dynamic model and b) the wells location

3.3 Data Evaluation

The previously described datasets exhibit notable differences regarding not only the spatial distribution but also the type of their containing data. Gullfaks static model extend throughout the whole Gullfaks field describing the stratigraphic layers belonging to the Upper Brent Formation. On the other hand, H1 dynamic model is placed on the southeast part of the Gullfaks field corresponding to a small section of the total field. Furthermore, H1 dynamic model and Gullfaks static model differ to the stratigraphic position on the field as the first one is located on the Lower Brent Formation.

Consequently, we could say that the Top Etive horizon represent the ‘contact point’ for the two datasets, as for the Gullfaks static model comprise the base while for the H1 segment dynamic model the top. In Figure 8, it is obvious that the top of the H1 dynamic model’s grid and Top Etive horizon of the Gullfaks static model do not match. The projection of the boundaries of the H1 dynamic model’s grid on the seismic data of the Gullfaks static model showed that they are inconsistence. This inconsistency could be explained by the fact that the interpretation of the external geometry for the H1 dynamic model was based on a different seismic dataset.

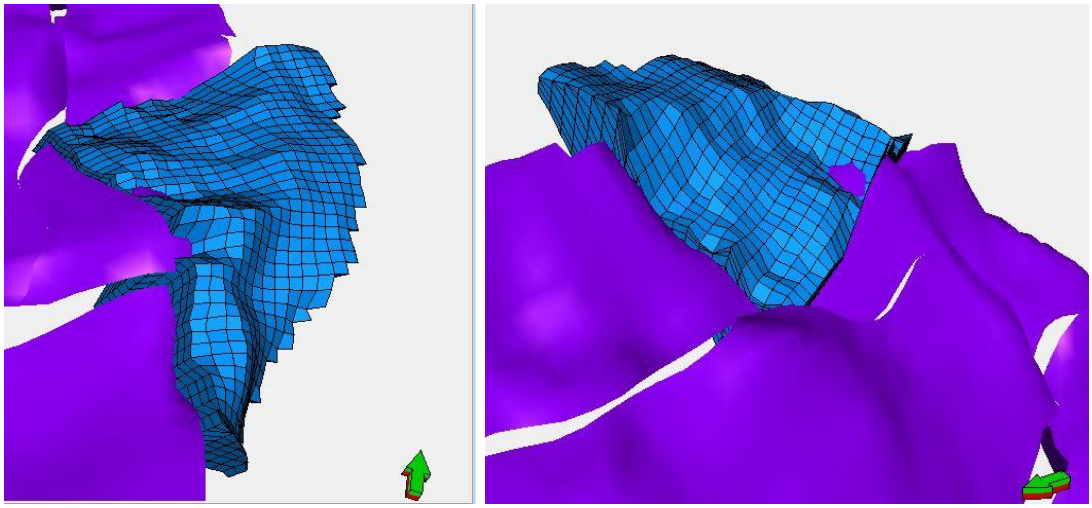

Figure 8 – The blue cells are the grid of the dynamic model H1 while the purple surface is the interpretation of Top Etive in the Gullfaks dataset. It obvious that the top of the grid is inconsistence with the surface of the Gullfaks dataset

Despite these spatial variations, the aforementioned datasets contained also different kind of well data. The 15 wells belonging to the Gullfaks static model dataset contained a complete series of logs such as permeability, porosity, gamma ray, net-to-gross, facies etc. On the contrary, only production/injection data were available for the wells of H1 dynamic model only. Another difference between the two group of wells were their spatial distribution because only the second group located inside the area of interest. Despite that the first group was useful to us for the interpretation of the seismic.

Regarding the lateral boundaries of H1 segment, the North and the West boundaries of the H1 dynamic model were vertical to the horizon planes but there is no evidence given by the seismic lines to justify the presence of these layer. The South and the East boundary are being determined by the wedge-like geometry of Lower Brent towards these directions.

3.4 Construction of the Static model

Every static model consists of two major parts; The structural framework and the property model. The structural framework is expressed by a 3D structural grid, and in practice on the one hand delimits the spatial extension of the model while on the other determines the resolution of the model by terms of the grid cell size. The property model constitutes by the filling of the structural framework with properties.

According Rivenæs et al (2010) the main elements in the model construction are (Figure 9):

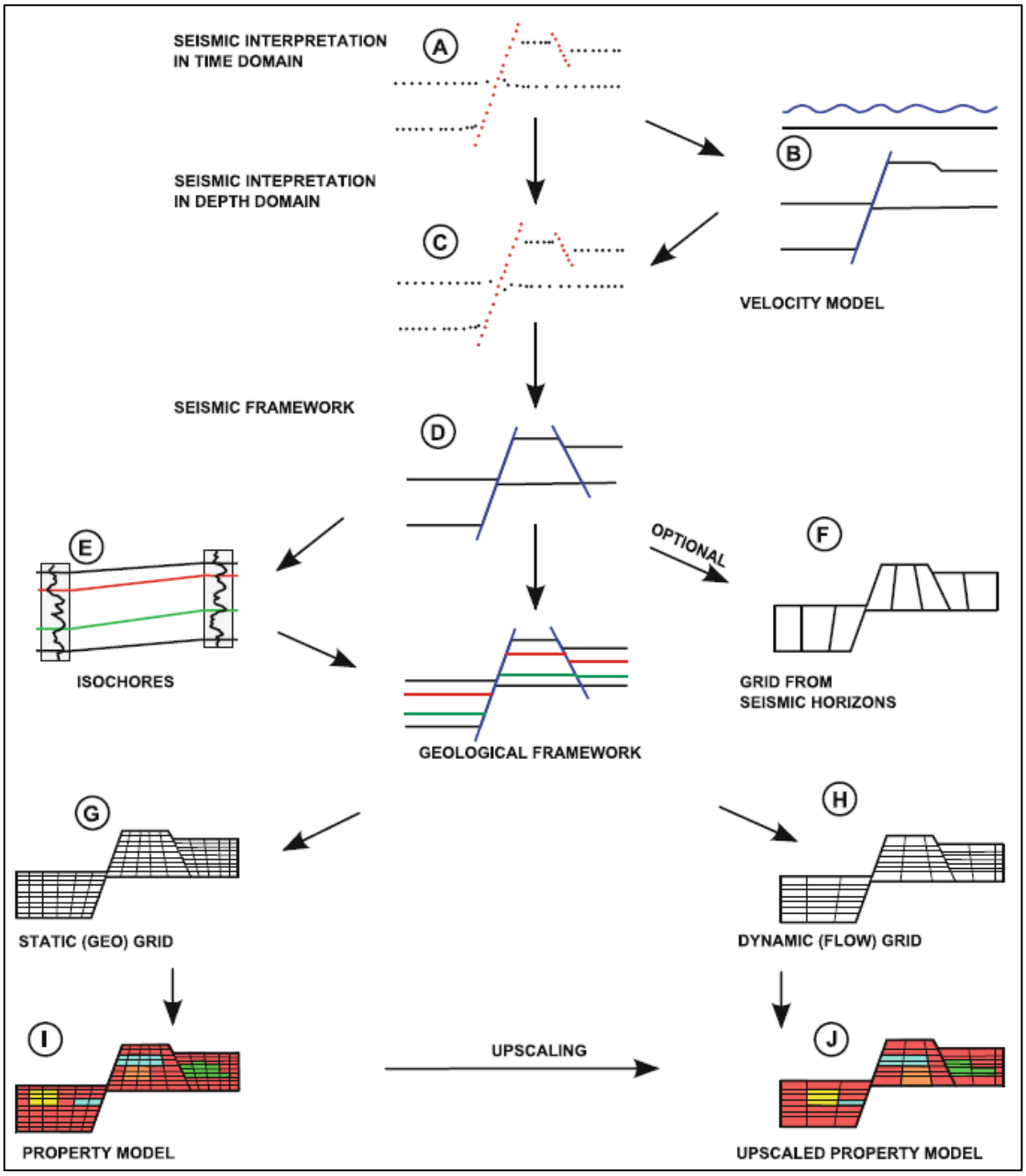

Figure 9 - Overview of a typical model construction work flow. Seismic interpretation is usually done in time domain and depthconverted (steps a–d). Isochore maps are made and merged with the seismic framework to make the geological framework (step e). An optional test grid may be made for quality control (step f). Based on this, two more 3D grids are made (steps g, h), which are filled with properties (steps i, j) ((*Rivenæs et al 2010*))

- Model the seismic horizons and faults. Seismic interpretation provides the most important input for building the gross skeleton of the reservoir, and make the seismic framework.

- As seismic resolution is limited, additional zones may be included from well log zonation and correlation, and the conceptual model. This refinement will outline the geological framework.
- Based on the geological framework, one or more 3D reservoir grids are constructed. In many cases a high resolution geological grid (also called static grid) is made, where the actual property modelling takes place, while a coarser flow simulation grid is constructed for the purpose of dynamic modelling.
- Property modelling is the step where each cell is assigned various petrophysical values (such as porosity, permeabilities and fluid saturations) and other values (such as facies and region identifiers).
- If both a high resolution static grid and a coarser flow simulation grid are generated, the process of transferring properties to the coarser grid is known as reservoir property upscaling.

For the present thesis, we construct an updated static model using the Petrel modeling software. This process is described in the next paragraphs and it could be subdivided in three stages. The first is relevant to the new interpretation of the stratigraphy and the tectonic for the area of interest. The second comprise the construction of a structural framework consistent to the new interpretation. Finally, the third step is the filling of this new framework with properties.

3.4.1 Reinterpreting horizons and faults

As reported in section 3.3 (Data Evaluation) there was the need to procced in a new interpretation of the seismic data. The new interpretation concluded 3 surface; Base Cretaceous, Top Etive and Lower Brent Base. To avoid misunderstanding concerning the nomenclature, the surface of the new interpretation will be mentioned as Base Cretaceous (new), Top Etive (new) and Lower Brent Base.

At the same time, we interpreted 5 new fault in the broader area of H1 dynamic model; North boundary fault, West boundary fault, en echelon Fault, Inner Fault 1 and Inner fault 2. These faults were not included in the initial interpretation of

the Gullfaks static model but as it shown in Figure 10, they exhibit more or less the same dip and angle of deep.

The key points of the new seismic interpretation were that:

- The boundaries of H1 dynamic model were inconsistence with the seismic
- The horizon Base Cretaceous (new), Top Etive (new) present only minor differences with the interpreted horizon in Gullfaks static model (Base Cretaceous and Top Etive respectively)
- A new interpretation for the Base of Brent
- Interpretation of new faults

Figure 11 represents the results of the new interpretation for two seismic lines in comparison with the interpretation of the Gullfaks static model and the boundaries of the H1 Dynamic model.

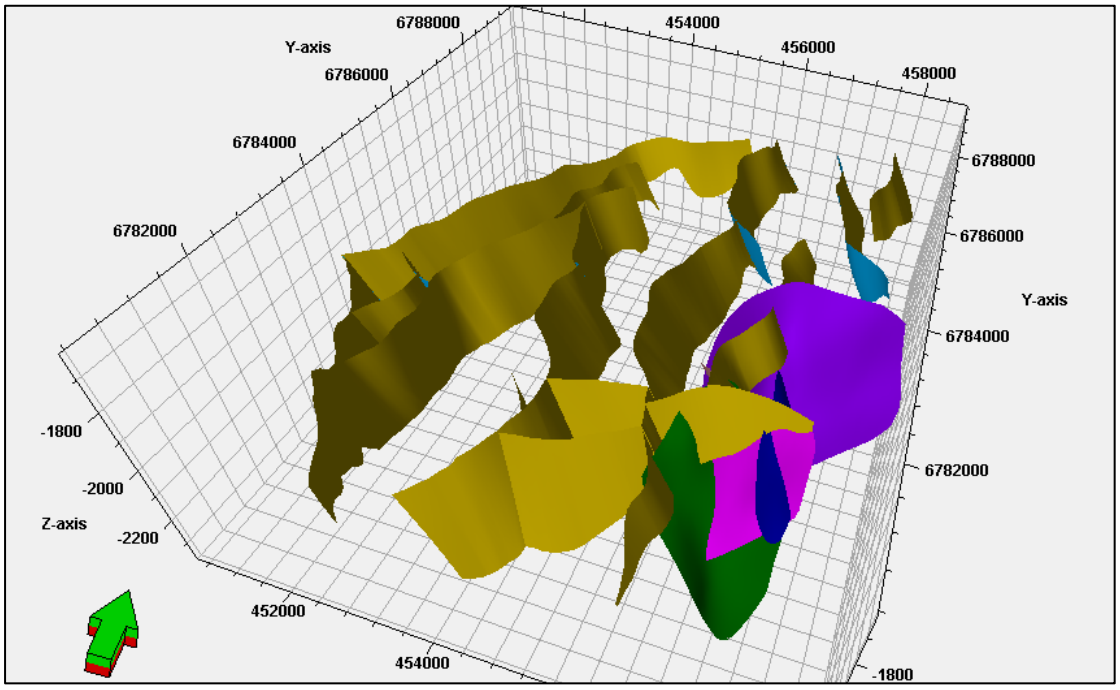

Figure 10 – The yellow planes represent the faults included in Gullfaks static model while the encolour planes the faults of the new interpretation. These two set of fault present similar dip an dip angle (z-exaggeration=5)

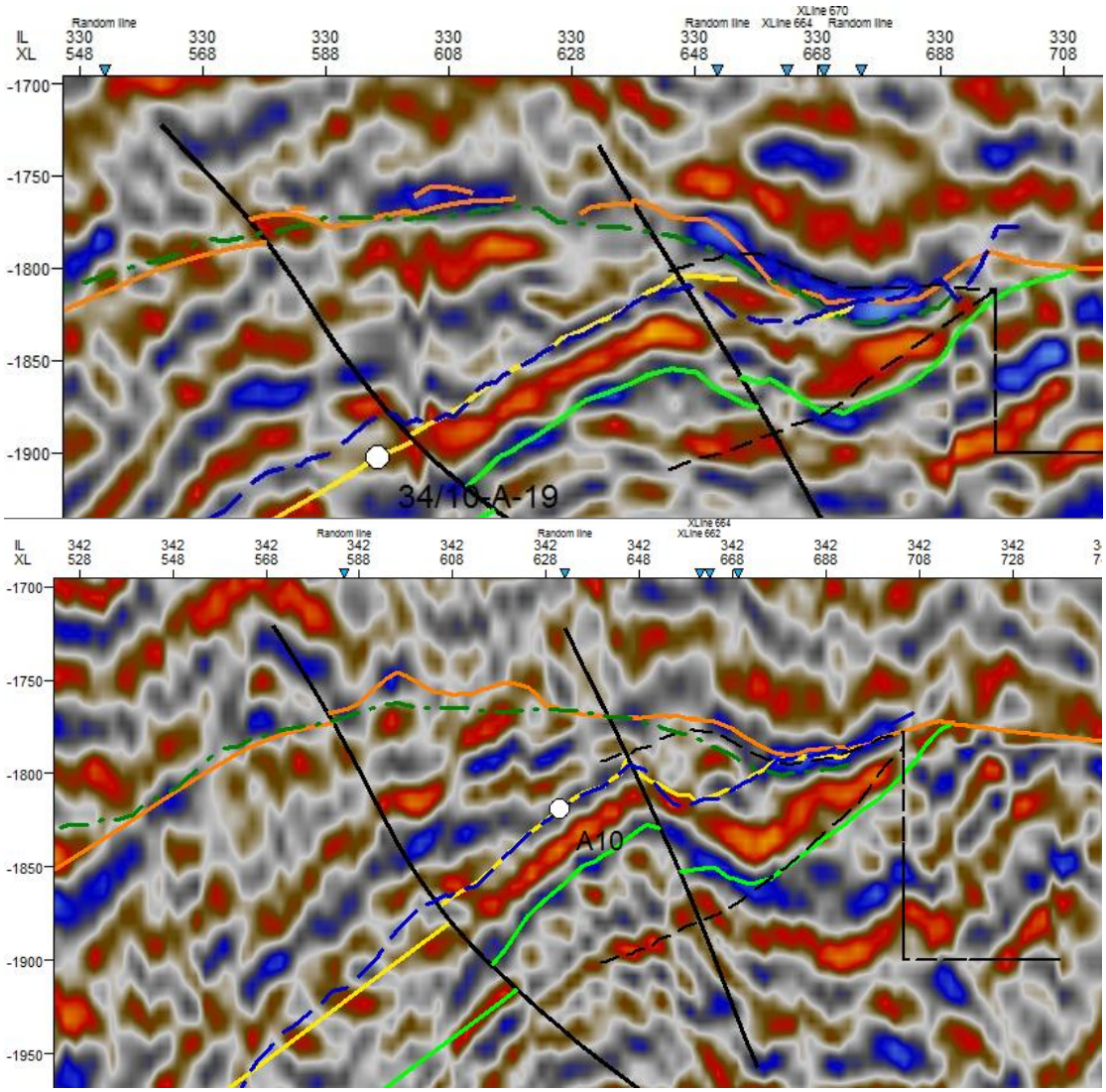

Figure 11 – The new interpretation on seismic inlines 330 (a) and 340 (b). With light green colour is represented the base Brent, with yellow the Top Etive (new), with orange the Base Cretaceous (new) while the black line represent the interpreted fault. The dusted green line represent the Base Cretaceous and the dusted blue Top Etive (Interepretaion of the Gulfaks Static model). Finaly the dusted black lines shoe the boundaries of H1 dynamic model

3.4.2 Structural framework

The construction of the static model's structural framework using Petrel involves two stage. The first one is using the available surfaces (stratigraphic horizon and faults) and creates space between them while the second divides the created space into cells.

In more detail for the first stage of constructing the structural framework in a Petrel environment the processes group *Structural Framework* was used. Firstly, we define the new framework and set the depth as the working domain (*New structural framework* process). Then, we introduced the interpreted faults

(*Fault framework* process) determining at the same time the relationship between them (Figure 12 a). At the same time the interpreted horizons (i.e. the Cretaceous Base (new), Top Etive (new) and Lower Brent Base) were introduced to the framework, with the Horizon modeling process. Finally, we procced to a rough limitation of the boundaries and the specification of the main spatial characteristics of the under-development framework (*Geometry definition* process).

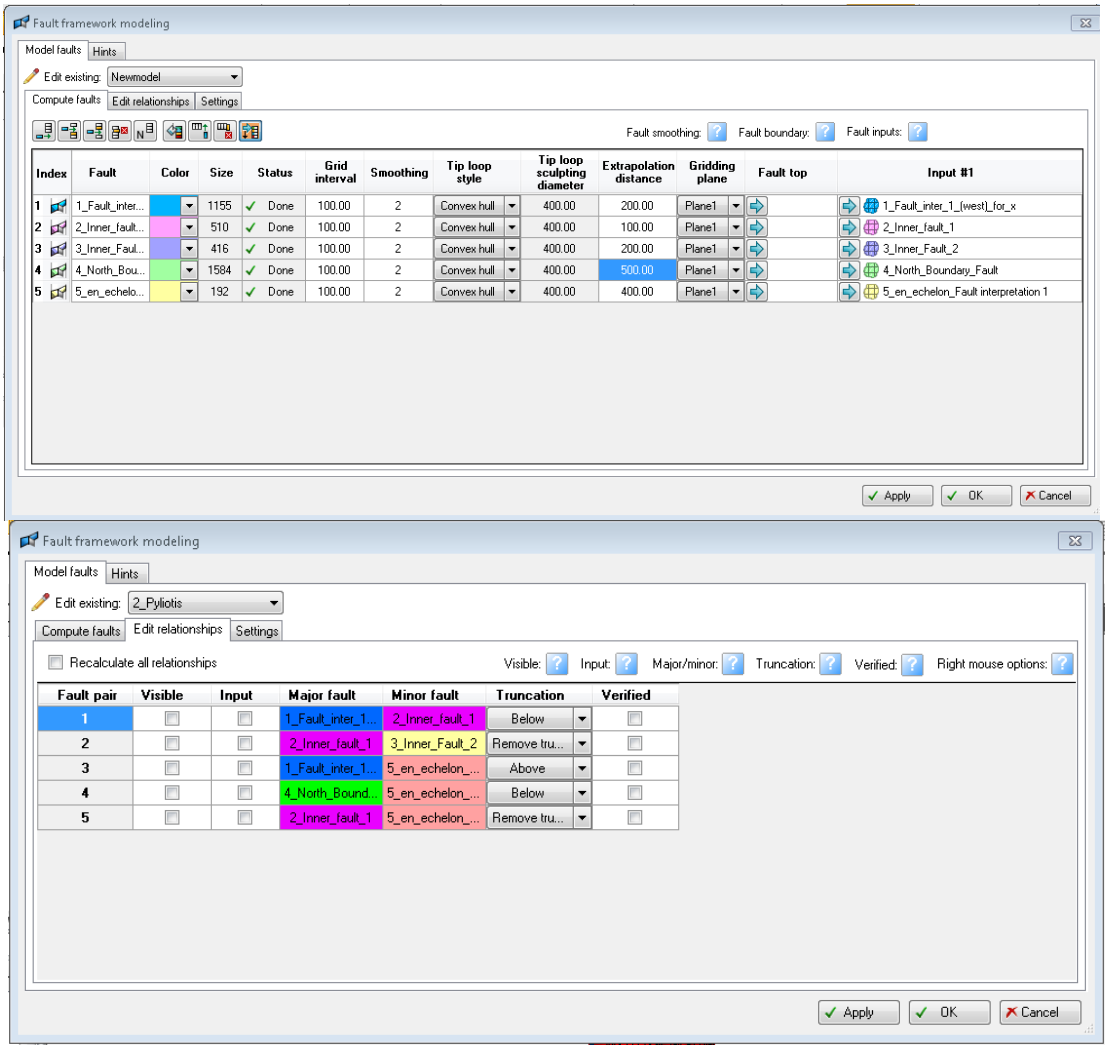

Figure 12 – a) fault framework modeling-import faults and their specification and b) fault framework modeling – relationship between the faults

At this point, the user has the ability of a first view regarding the relationship of horizon and faults (Figure 13). In cases where the result isn't covenant with the broader geological interpretation of the area, or inconsistences between the surface and the faults occur, or even one of the produced surfaces displays unnatural shapes, the previous steps can be repeated changing the various parameters described previously or even there is the possibility to revise the

initial interpretation. When the result is satisfying, the box named refine and create zone model in the Horizon modeling process is checked in order to ‘fill’ the space between the horizon and the faults which were used. The result is the creation of zones between the faults and the horizons (Figure 14).

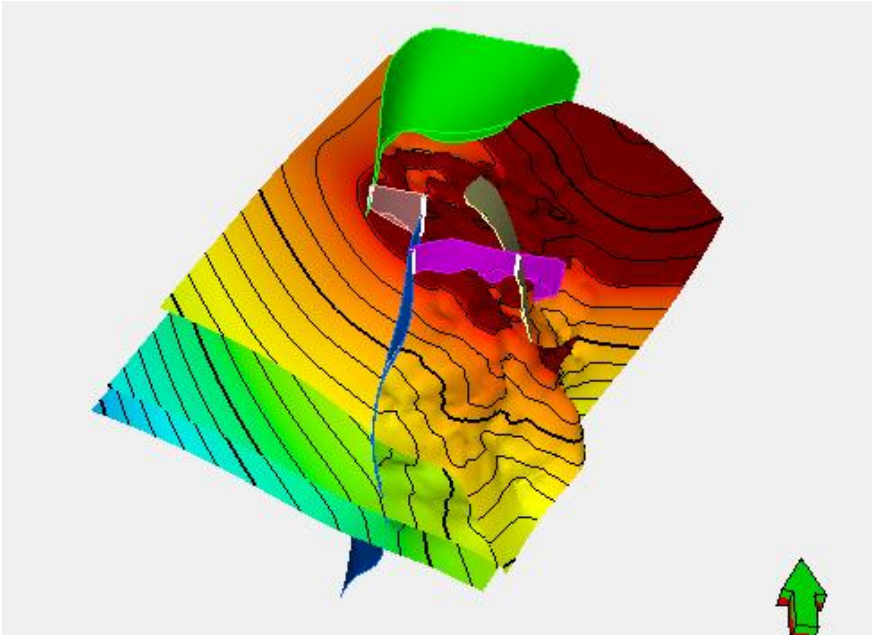

Figure 13 – The relationship between the surfaces and fault produced with structural framework process

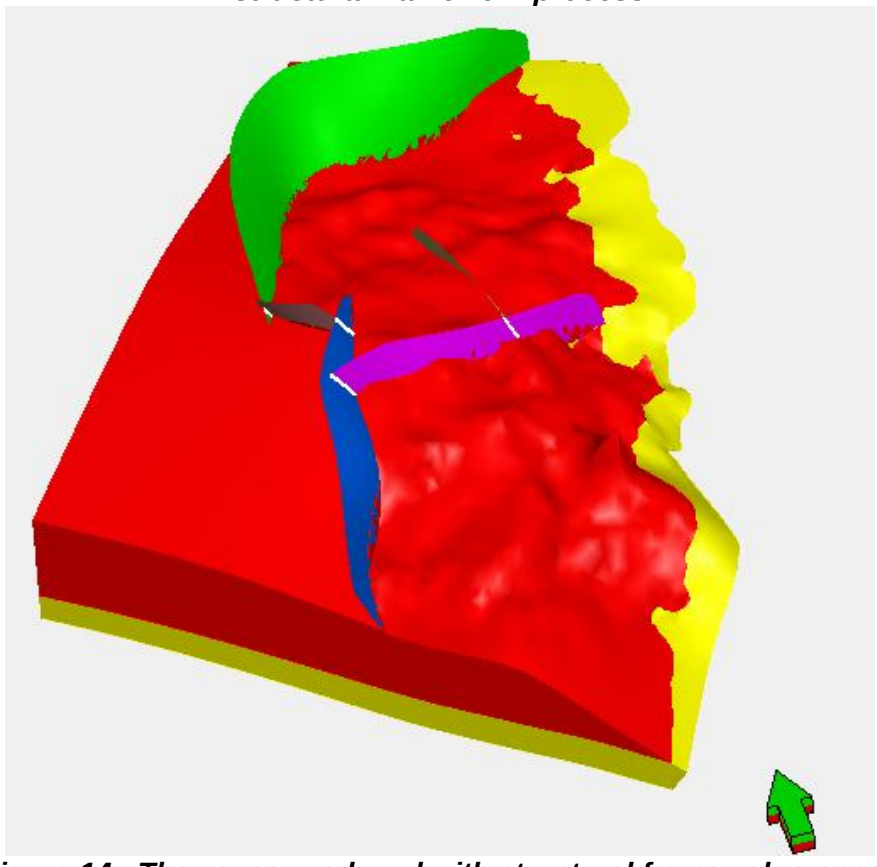

Figure 14 - The zones produced with structural framewok process

After the creation of the zones, we used the Structural gridding process to divide them into cells. We defined the horizons and faults participating in the new model and the number of the layers and the pattern of filling each zone, as well as the size and the orientation of the cell. The grid cell size used selected to have half of the length in each direction comparing to the cell size of the H1 dynamic model. So, the dx and dy length of the cells specified at 25m while dz was controlled by the number of layer (20) which filled the zone corresponding between Top Etive and Lower Brent Base giving a mean value of 3.5 m. The azimuth of the grid orientation set up to 350^{o}, in order to be parallel with the strike of the main fault of the study area.

The resulted grid is presented in Figure 15.

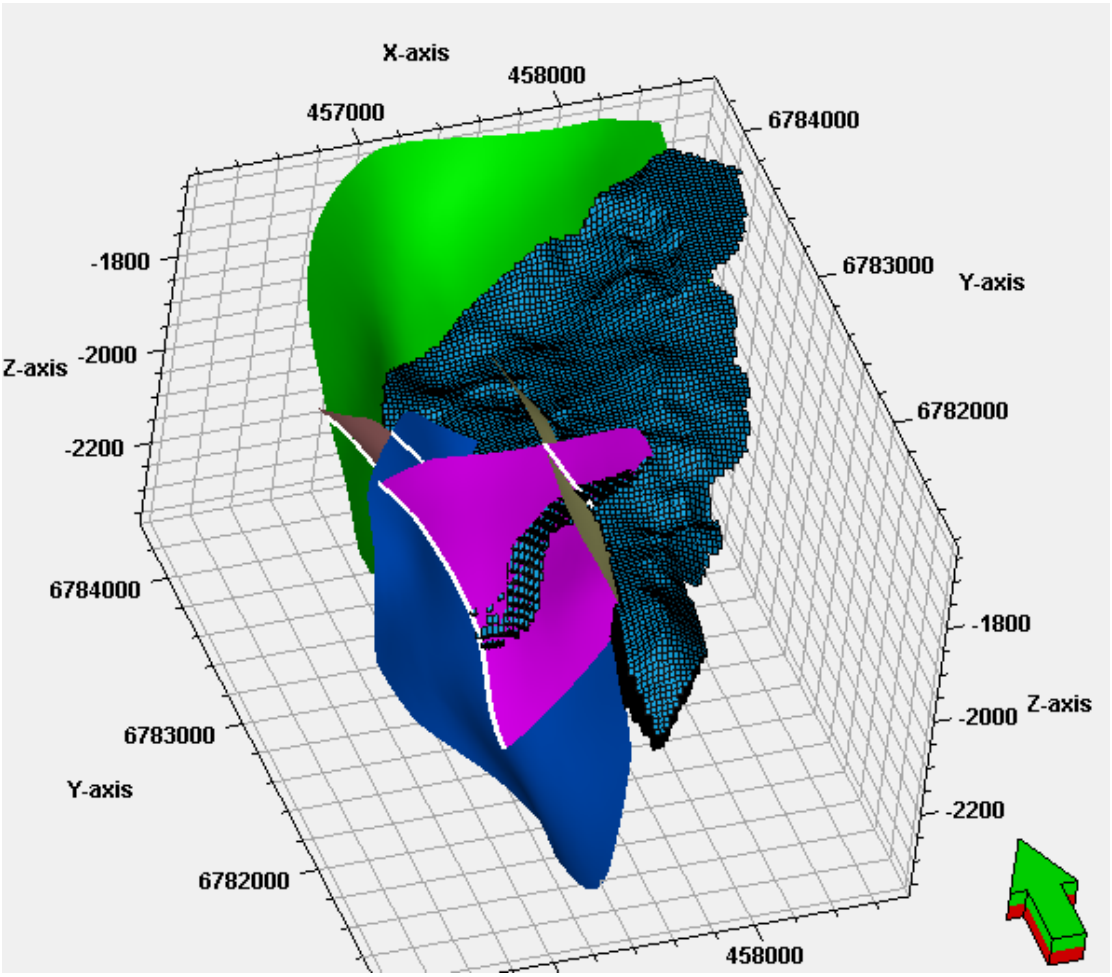

Figure 15 – 3D view of the updated structural grid

The spatial extend of the new grid compared to the H1 dynamic model's grid exhibit major differences. This differences concern both in the horizontal

extension and the vertical thickness of the model (Figure 16 and Figure 17). New model's vertical thickness was smaller but comparable with the one of the initial model. On the other hand, the horizontal extension of the new model was significantly larger.

So far, there was no data indicating the lateral extend of our model. This was not a problem for the southwards and eastwards boundaries as they controlled by the wedge geometry of the studied formations (this was also the case for the H1 dynamic model). The northwards and westwards boundaries in the H1

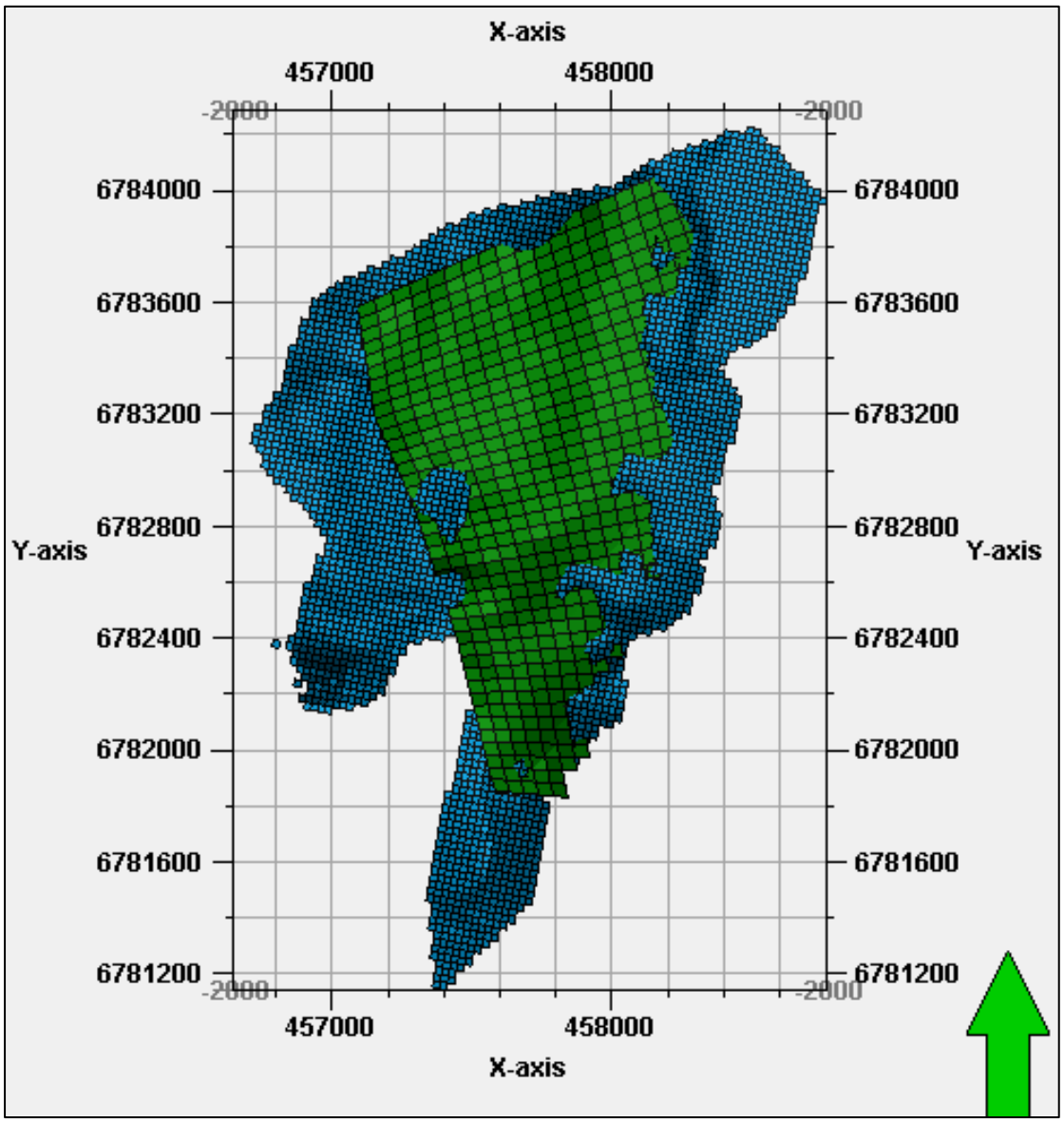

Figure 16 – Differences on the horizontal extension of the updated structural grid (blue cells) and H1 dynamic model's grid (Top view)

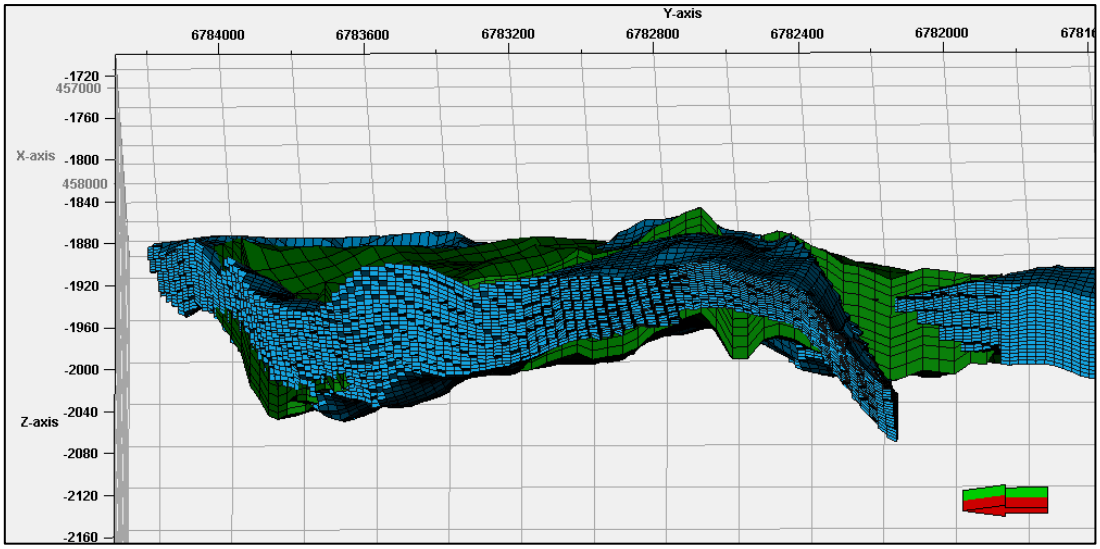

Figure 17 - Differences on the vertical extension of the updated structural grid (blue cells) and H1 dynamic model's grid (East view-z scale exaggeration=3)

dynamic model were vertical planes. These planes show no possible correlations with the seismic data, so it was completely unclear how they have been created (probably from production data).

It is not rare that during the seismic interpretation some structure not to be recognized. Tollefsen et al (1992) has reported for the study area that the 70% of the wells prove minor or large faults not previously seen on seismic. Consequently, we revisit the seismics and we notice that in the broader area North side of the West boundary the top surface of our model (top Etive (new)) (Figure 18 a) and bottom surface (Lower Brent Base) exhibit some similar changes in their depth (Figure 18 b). This change could be explained by a structure (for example a fault) which wasn't detected during the seismic interpretation.

Base on the aforementioned uncertainties regarding the north part of the west boundary and for comparison reasons, in the present thesis another two grids will be used. The first one confined the model to the possible sub seismic structure and the other one to the limits of the H1 dynamic model. The three grid will be referred from now on as:

Grid I - the initial grid

Grid O - the initial grid bounded based H1 dynamic model

Grid S - the initial grid bounded to the sub-seismic structure

The confinement of the initial grid in order to produce grids O and S held by setting zero permeabilities to the cells being cut from the respective surfaces (see details in 3.4.3 Property modelling).

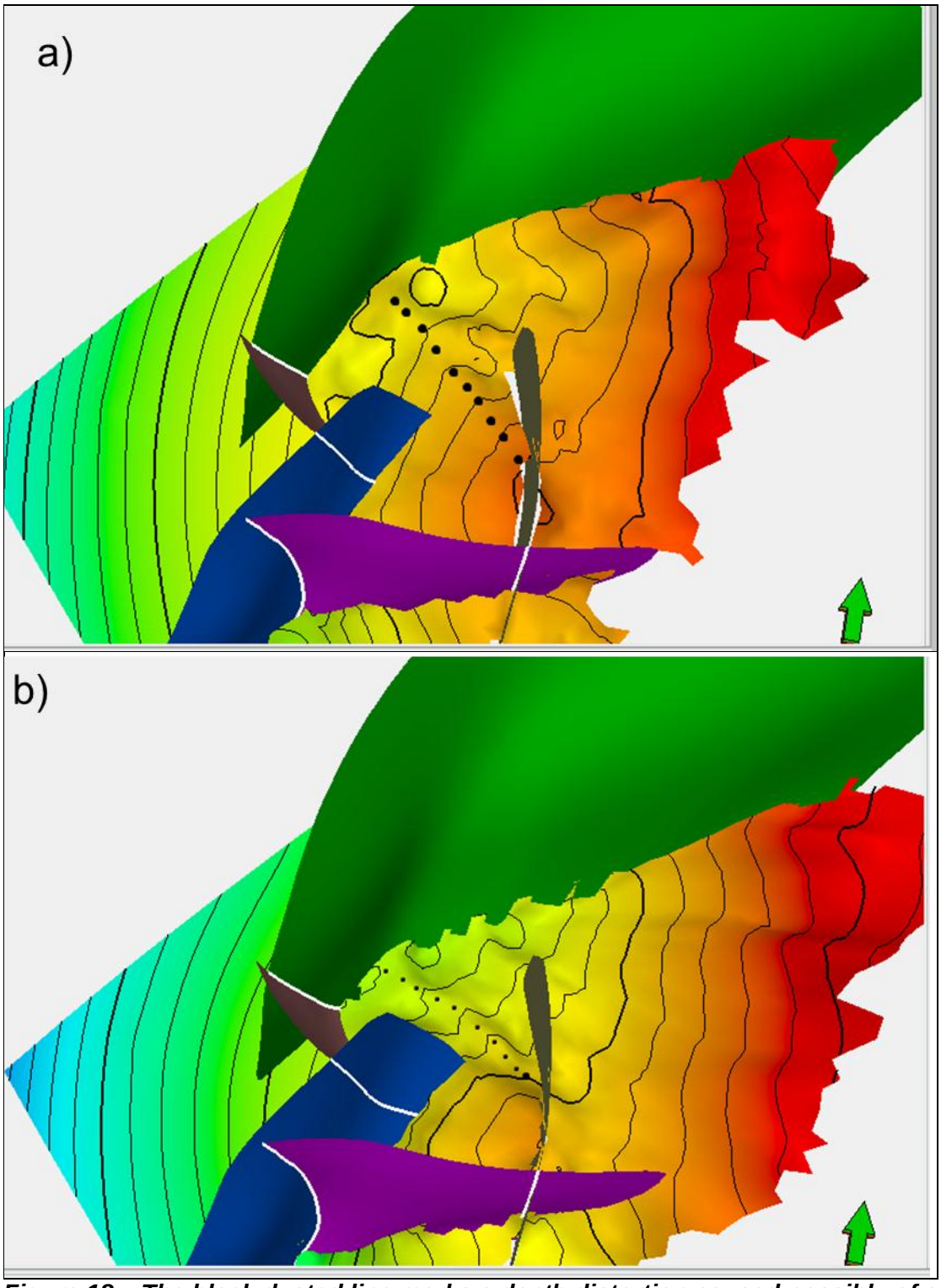

Figure 18 – The black dusted line marks a depth distortion caused possibly of a sub-seismic structure both on Top Etive (new) surface (a) and Base Brent surface (b)

3.4.3 Property modelling

After constructing a grid, it is essential to be filled with properties. A common practice is to use the available well log data. The well log data are generated by constant recording using the logging tools, producing this way depth relative curves for each property. Because the grid cells are much larger than the well logs density, well log data must be scaled up before they assigned to the grid cells. Scale up (or blocking) well logs is the process of assigning well log data to grid cells. In the model, each grid cell has a single value for each property (porosity, permeability, etc). (petrofaq.org).

As already reported the located inside the studied area wells lack of any kind of well logs. Consequently, the only data available regarding porosity, permeability and net-to-gross were the values assigned to the cells of H1 dynamic model.

For the purpose of this thesis, we extract these values along with their coordinates for the cells were penetrated by wells. These data were imported to petrel as *Petrel point with attributes (ASCII)* file. Afterwards using the Scale up well logs process (Property modeling) we assign these values to the corresponding cells creating this way pseudo-upscaled values (Figure 19).

At this point we should notice that on the H1 dynamic model:

a) The permeabilities for y-direction were set equal to the x-direction permeabilities
b) the permeabilities in z-direction had been changed by using multipliers resulting low values. The result was that z-permeabilities exhibit extremely low values (Figure 20)
c) net-to-gross values were set by layer (Table 1)

The next step was to distribute the values to the whole grid (Petrophysical modeling process). There are many algorithms available in Petrel for the petrophysical modeling. In the content of this thesis we use the two most common of them; Kriging and Gaussian random function. Additional to these two algorithms and because z permeabilities values were too small we also expressed as a ratio of the horizontal permeability produced by the

aforementioned two algorithms. Thus, we end up with four different methods regarding petrophysical modeling:

- Krigging (Figure 21)
- Gaussian random function simulation (Figure 22)
- Krigging for all properties, and permeabilities in z direction equals to the one tenth of permeabilities in x direction
- Gaussian random function simulation for all properties, and permeabilities in z direction equals to the one tenth of permeabilities in x direction.

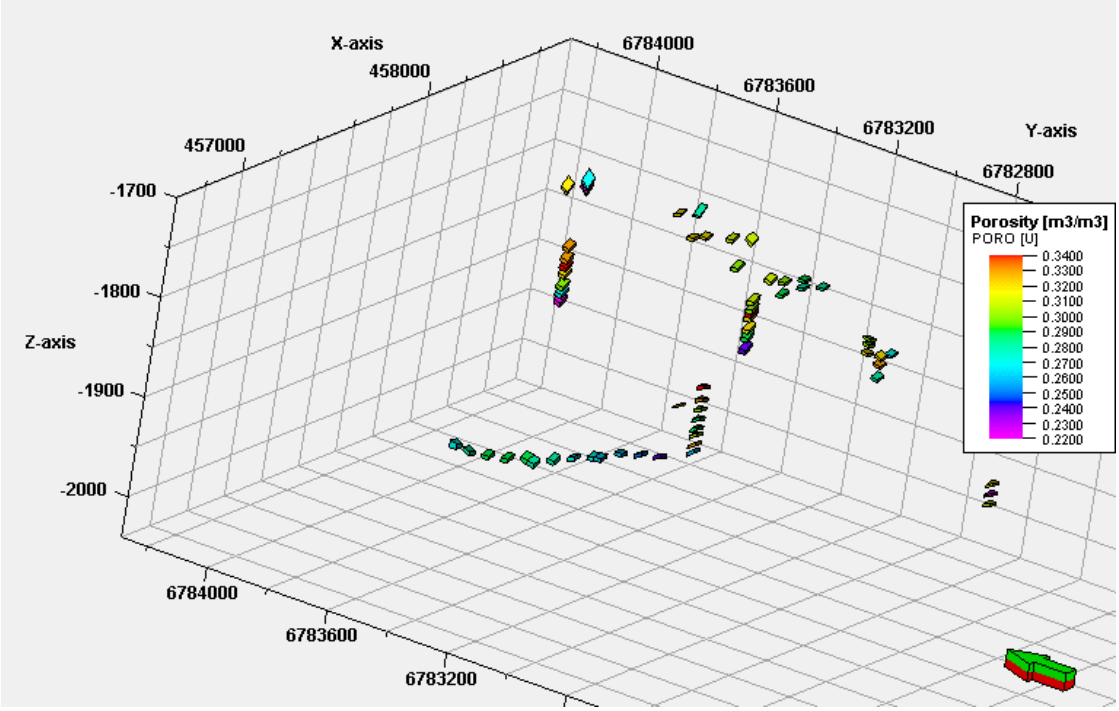

Figure 19 - Graphical represantation of the pseudo-upsceled introducted values of porosity for the grid I

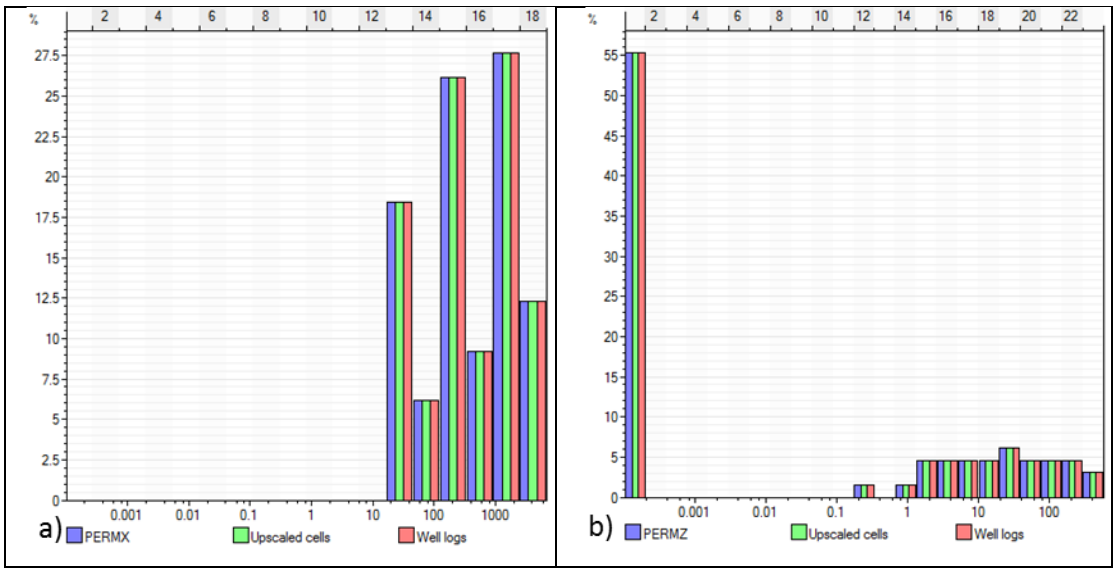

Figure 20 – Distributions of the permeability x (a) and the permeability z (b) as introduced to cells being penetrated by wells. Since there not well data the well log data and the upscaled data are equal

Table 1 – H1 dynamic model's net-to-gross values by layer

K index	Net-to-gross
1, 2	0.19
3	0.96
4, 5	0.98
6	0.90
7, 8, 9	0.96
10	1.00
11, 12, 13	0.90

These four types of distribution combined with the 3 different grids (I, O and S see details in 3.4.2 Structural framework) resulted in the construction of 12 different static model. The nomenclature of these models is present in Table 2.

At this point we should report again that the confinement of the grid was held by setting zero permeabilities to the cell being cut by the different boundaries (Figure 23). Regarding the two faults crosscutting all of the three grid (inner fault 1 and 2) only inner fault 2 considered to be an impermeable barrier. This was because the set up of inner fault 1 as an impermeable barrier would have cause an isolation of well P-A35.

Table 2 – Nomenclature for the 12 constructed model

	New grid	barrier at the possible structure	barrier at the area of the initial west boundary
Kriging	IK	SK	OK
Gaussian random function similutation	IG	SG	OG
Krigging and permz=0.1*permx	IK10	SK10	OK10
Gaussian random function simulation and permz=0.1*permx	IG10	SG10	OG10

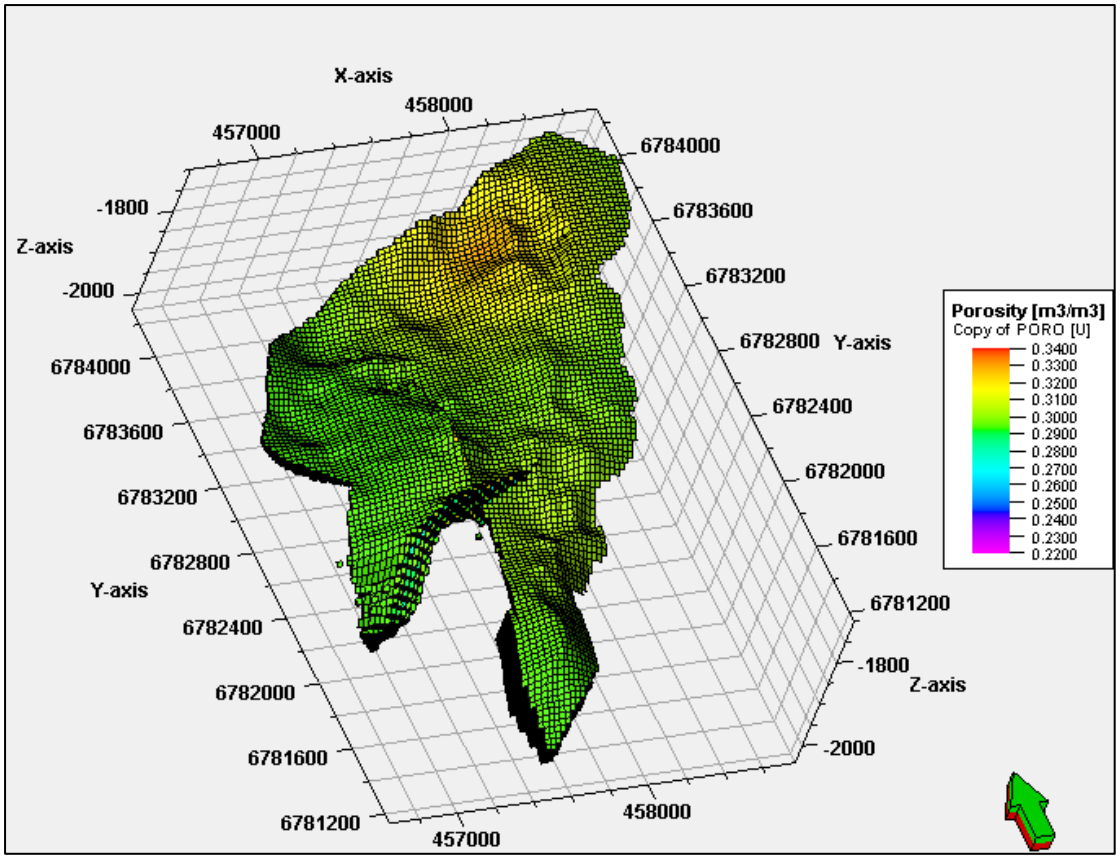

Figure 21 - Porosity values of the Grid I using Kriging algorithm

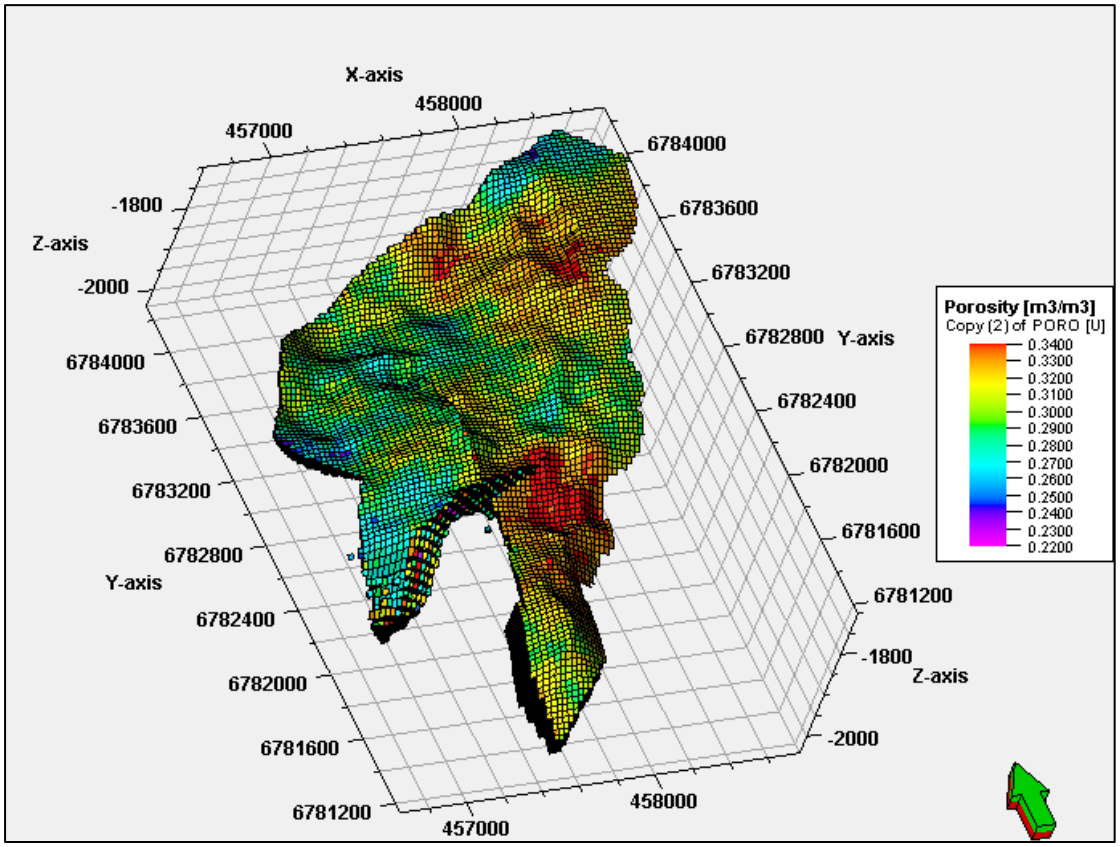

Figure 22 - Porosity values of the Grid I using Gaussian random function simulation algorithm

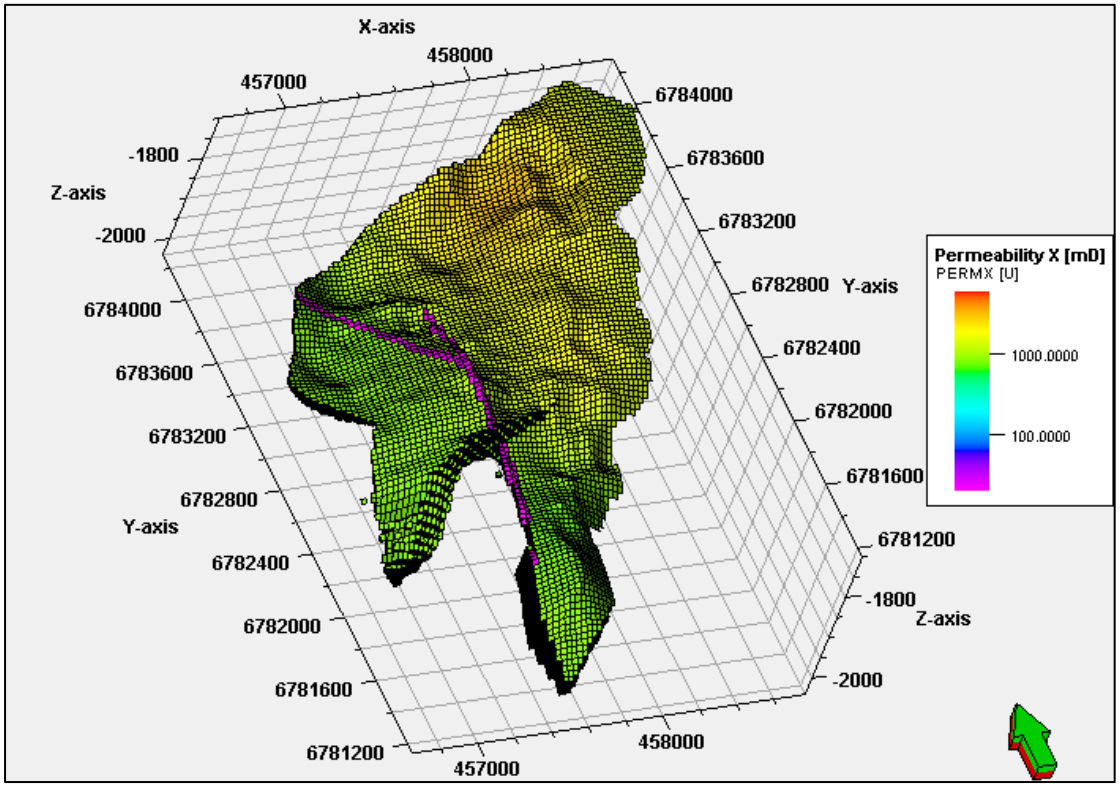

Figure 23 – Permeability-x values of the Grid S using Kriging algorithm

3.5 Construction of the Dynamic model

The construction of a dynamic model could take placed by incorporating to the static model relevant data to the containing fluid of the reservoir such as relative permeabilities, PVT data, or production data in already operating fields. In many case, static model subjects to modifications if needed. The reason for such modification could be the upscaling of grid because the initial grid was very fine (small cell size) for representing accurately the geological complexity of a reservoir costing this in computational time. In other cases, the initial grid can be modified nearby the wells.

Another extra characteristic of the dynamic models is that they deal with cell-face properties. The meaning of this that in dynamic modeling isn't enough to set cell center values to the grid cells but the connectivity of the cells should be computed.

The final purpose of a dynamic model is to simulate the behavior of a reservoir. So, in order to check the efficiency of the dynamic model a comparison of the models prediction with the production data is made. The procedure of

calibrating the model until it closely reproduces the past behavior is called history matching. Rivenæs et al 2010 describes two ways of history matching (Figure 24):

1. The inner loop. After the model, has been upscaled from the static model, the reservoir engineer adjusts the flow simulation model in order to match model with production data. For example, the reservoir engineer may suggest that the permeability should be multiplied with a factor ten in selected areas to improve match.

2. The outer loop. In this case the reservoir engineer works together with the geomodeller to modify the static model that provides input to the dynamic model.

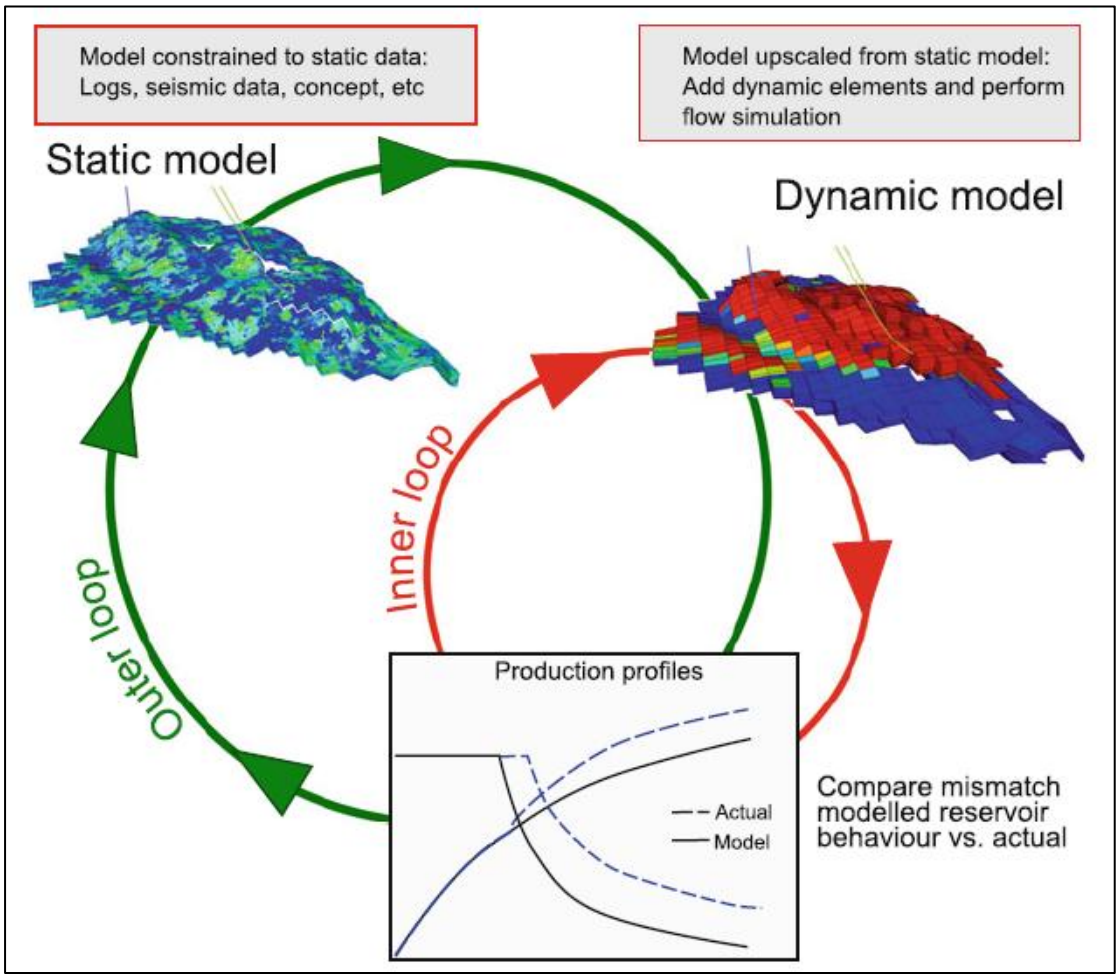

Figure 24 - History matching loop. Modelled dynamic behaviour is compared with actual, and calibration of the model may be done in the dynamic model directly (inner loop) or the static model (outer loop)

3.5.1 Eclipse simulator

As reported previously (3.4.2 and 3.4.3) a total of 12 static models was constructed. These models were the result of combining 3 different structural grids with 4 methods of property propagation. As many dynamic models were constructed.

In the present thesis, the construction of dynamic models as well as the calibration of the constructed models (history matching) held with the use of the Eclipse simulator (by Schlumberger service company). In general, the data files compatible with the Eclipse software have an ASCII text format and comprise by a series of command which are included in eight sections; namely *RUNSPEC, GRID, EDIT, PROPS, REGIONS, SOLUTION, SUMMARY* and *SCHEDULE* (Figure 25). Out of these sections *EDIT, REGIONS* and *SUMMARY* are optional while the rest sections are required.

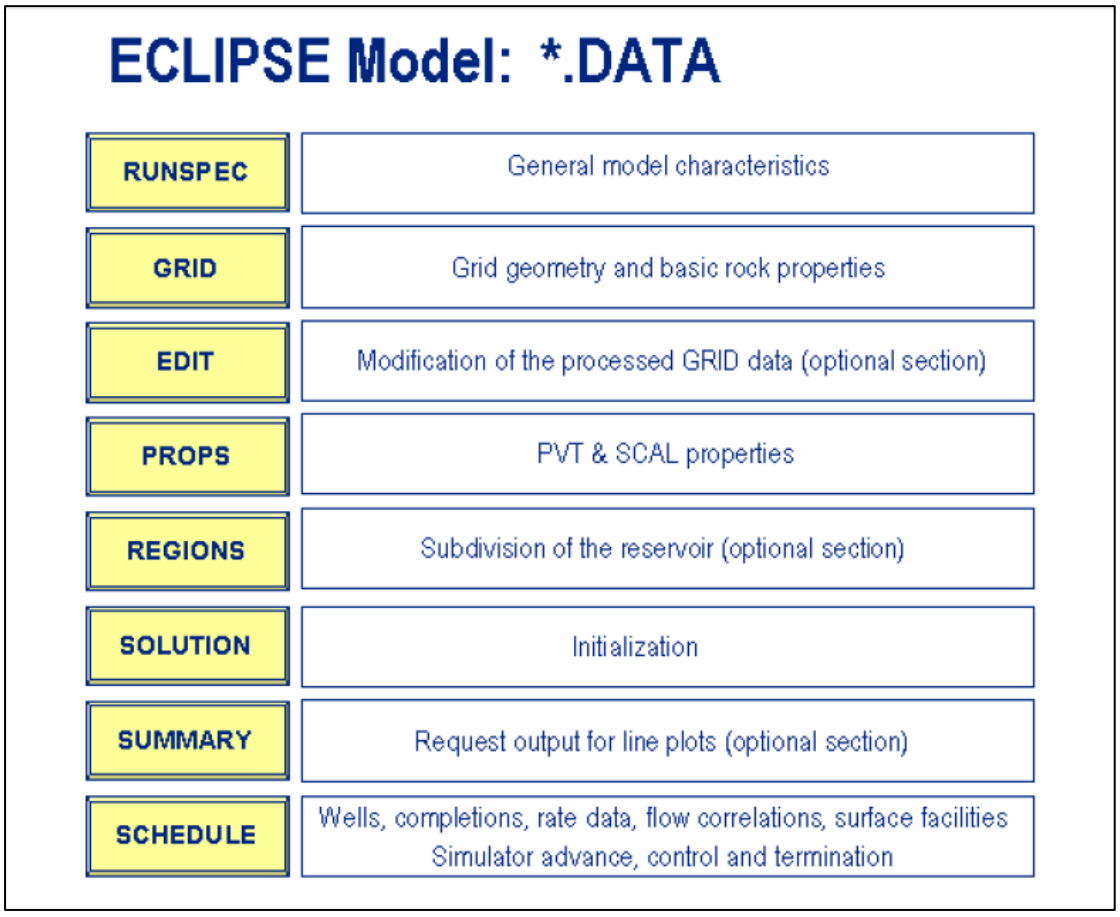

Figure 25 – Eclipse Model (Eclipse blackoil2007)

3.5.2 Evaluation of the constructed dynamic models

The 12 constructed dynamic models were evaluated qualitatively to be determined which of them produce closer to the history data predictions. The performance of the different models evaluated based on the accuracy of well water cut predictions. Initially it was determined the grid (I, O or S) which performed better. For every property distribution, the well water cut predictions produced by the different grids projected in relevance with the observed history data.

Table 3 shows the summarized results of this evaluation. In Figure 26 to 45 corresponding charts are presented. Based on these result the I grid performed better in the most cases.

Afterwards, in a similar way (Table 4, Figure 46 to 50) it was concluded that grid I performs better when the property distribution method K10 is applied.

Therefore, based on our evaluation model IK10 considered to be the model with the most valid predictions.

Table 3 - Comparative evaluation of the 3 different grids relatively to the method of property distribution based on the total well oil production (WOPT)

	K	G	K10	G10
WOPT -PA17	I	I	O	O
WOPT-PA1H	S	I	O	S
WOPT-PA2AH	I	I	I	I
WOPT-PA35	S	I	S	I
WOPT-PA39	I	I	I	I

Table 4 - Comparative evaluation of the methods of property distribution for structural grid I based on the total well oil production (WOPT)

	Distribution method
WOPT -PA17	K10
WOPT-PA1H	G
WOPT-PA2AH	K10
WOPT-PA35	G
WOPT-PA39	K10

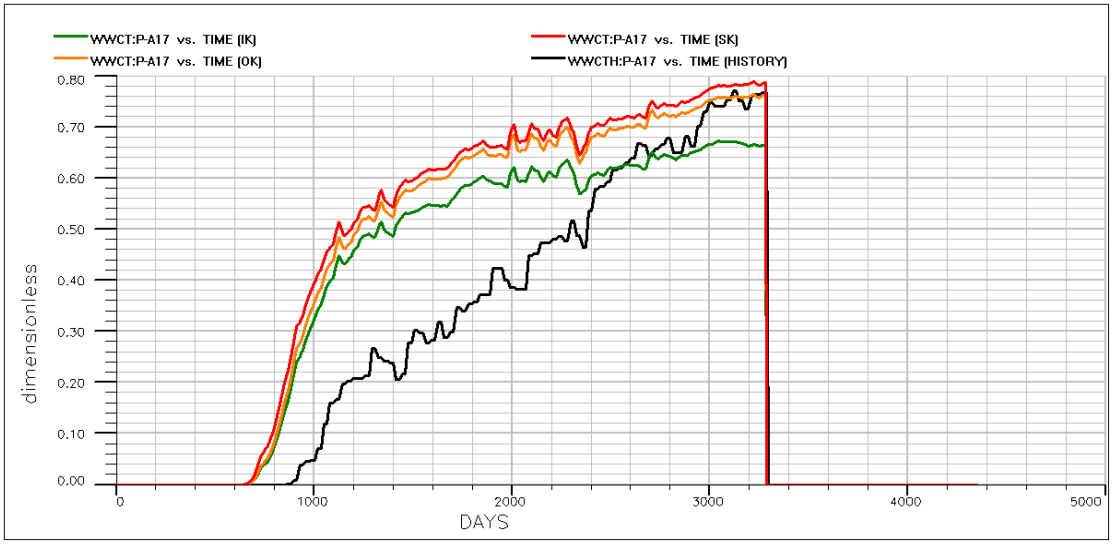

Figure 26 - Comparative chart of the predicted by the models IK, OK and SK well water cut (WWCT) of P-A17 well with history data

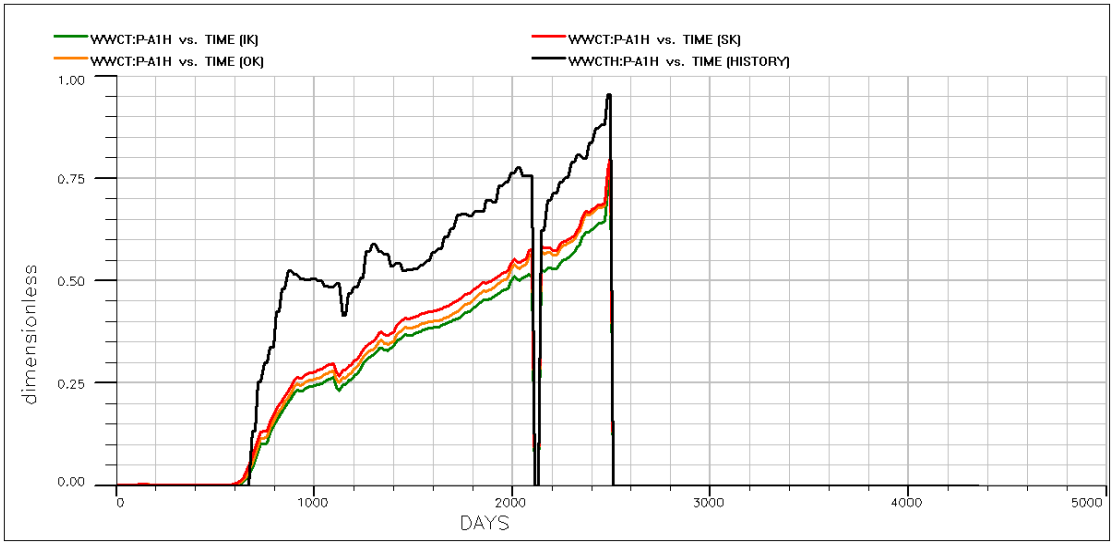

Figure 27 - Comparative chart of the predicted by the models IK, OK and SK well water cut (WWCT) of P-A1H well with history data

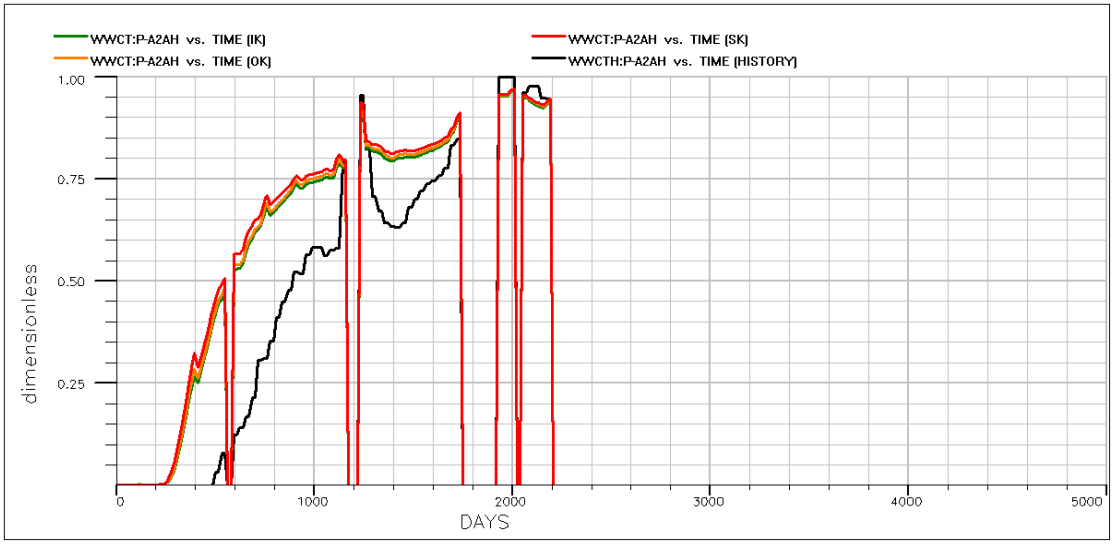

Figure 28 Comparative chart of the predicted by the models IK, OK and SK well water cut (WWCT) of P-A2AH well with history data

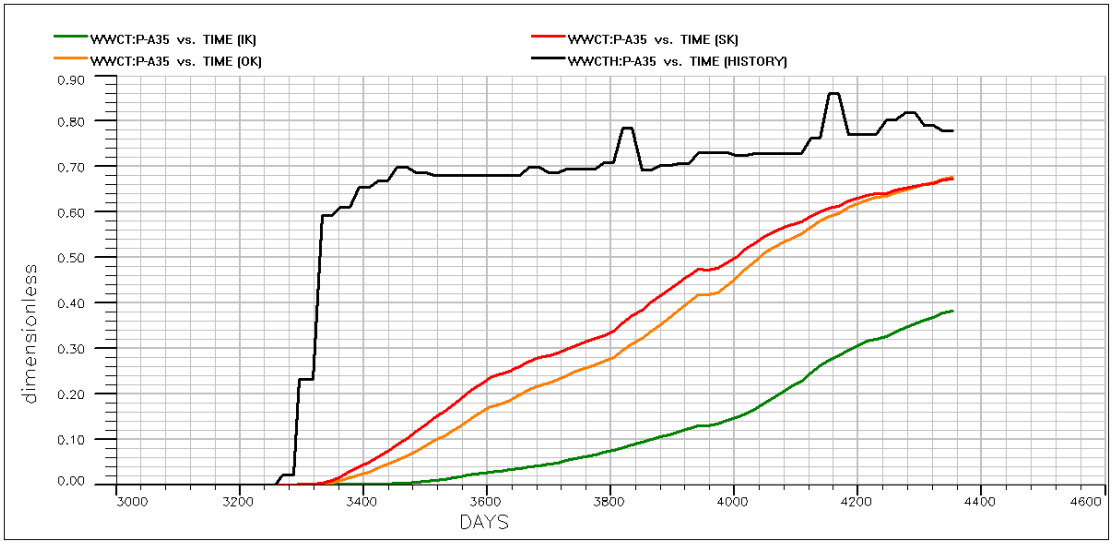

Figure 29 - Comparative chart of the predicted by the models IK, OK and SK well water cut (WWCT) of P-A35 well with history data

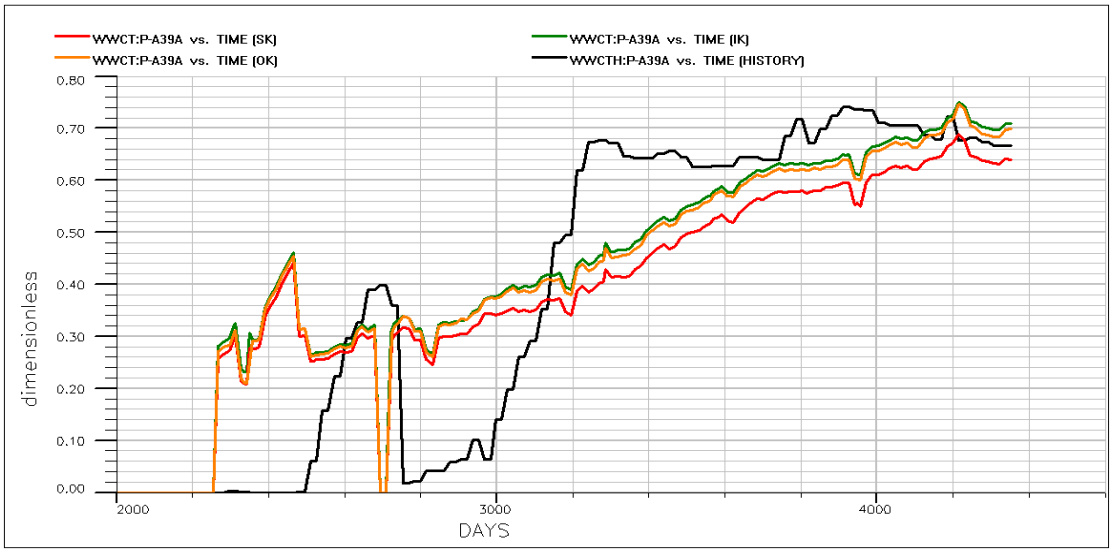

Figure 30 - Comparative chart of the predicted by the models IK, OK and SK well water cut (WWCT) of P-A39A well with history data

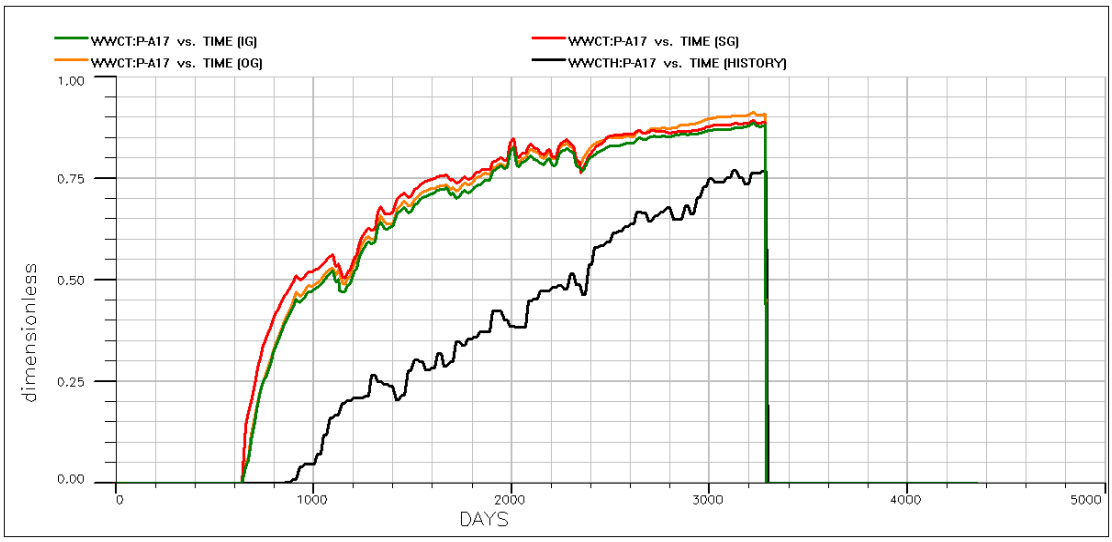

Figure 31 - Comparative chart of the predicted by the models IG, OG and SG well water cut (WWCT) of P-A17 well with history data

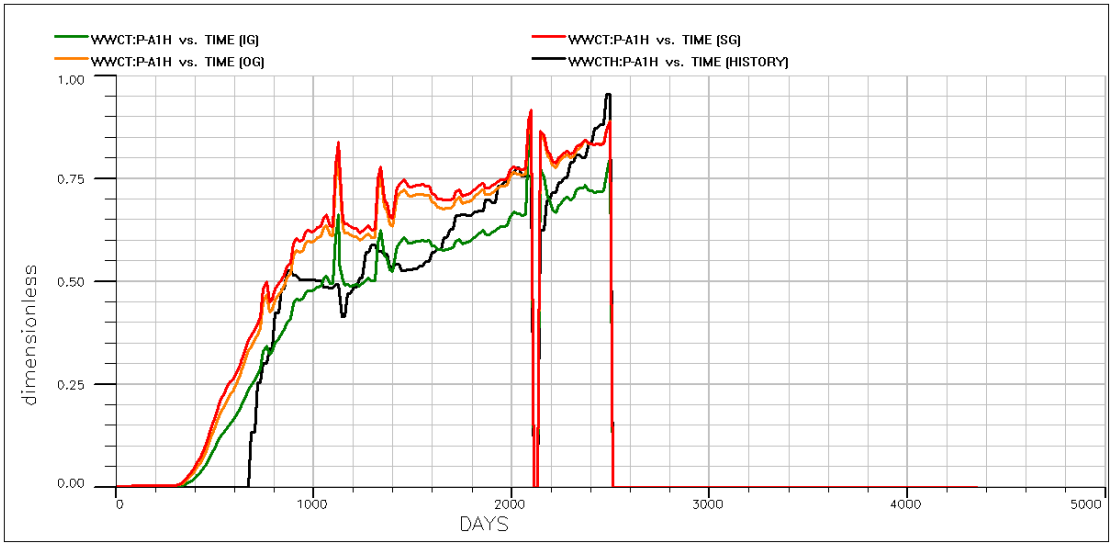

Figure 32 – Comparative chart of the predicted by the models IG, OG and SG well water cut (WWCT) of P-A1H well with history data

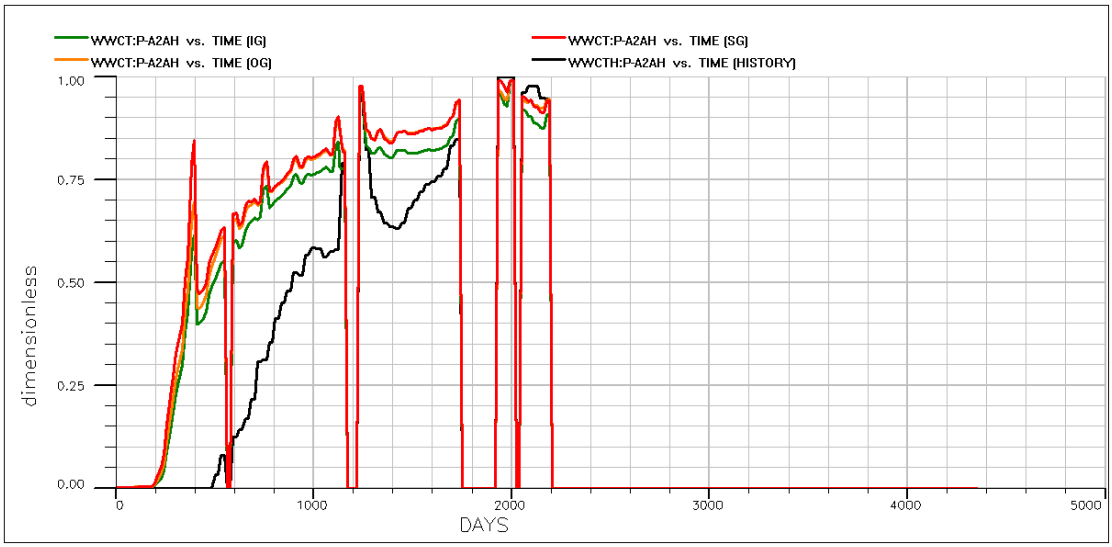

Figure 33 – Comparative chart of the predicted by the models IG, OG and SG well water cut (WWCT) of P-A2AH well with history data

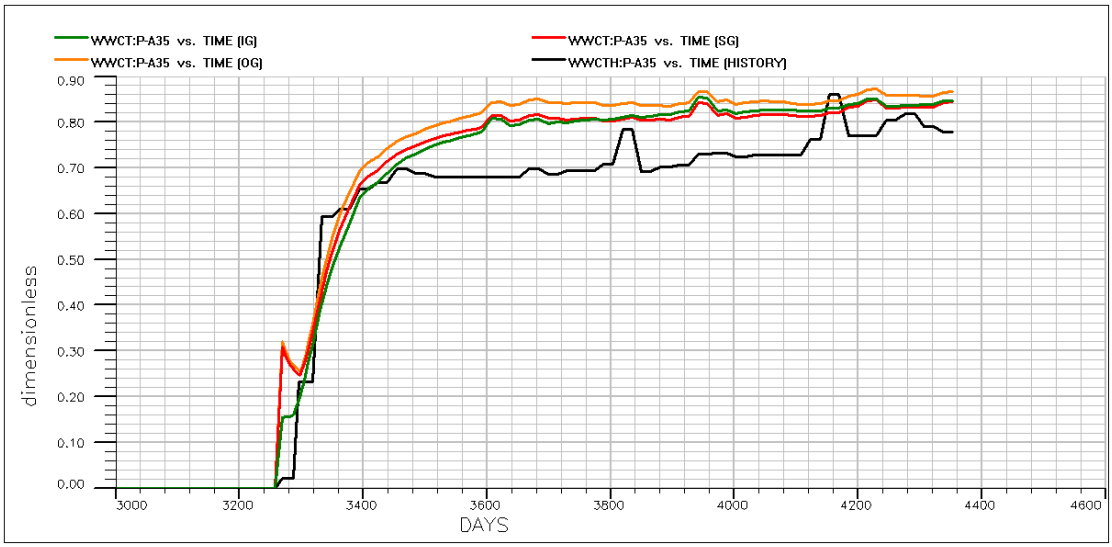

Figure 34 - Comparative chart of the predicted by the models IG, OG and SG well water cut (WWCT) of P-A35 well with history data

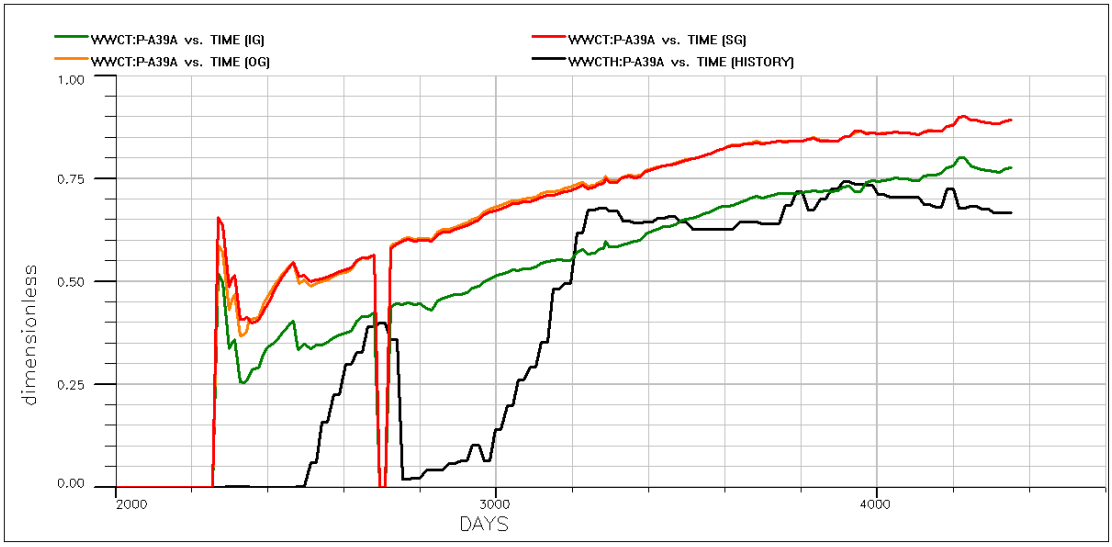

Figure 35 - Comparative chart of the predicted by the models IG, OG and SG well water cut (WWCT) of P-A39A well with history data

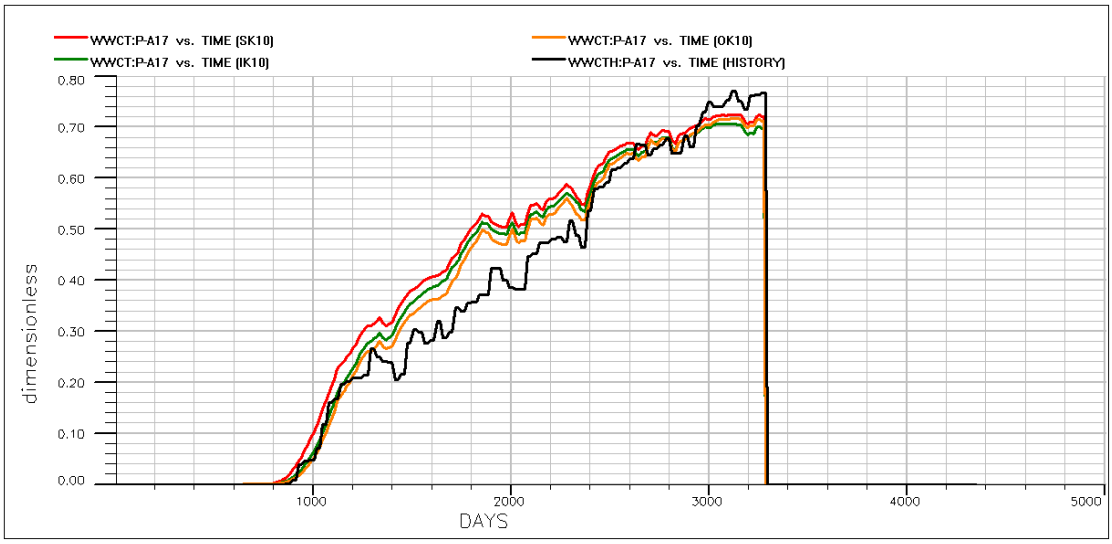

Figure 36 - Comparative chart of the predicted by the models IK10, OK10 and SK10 well water cut (WWCT) of P-A17 well with history data

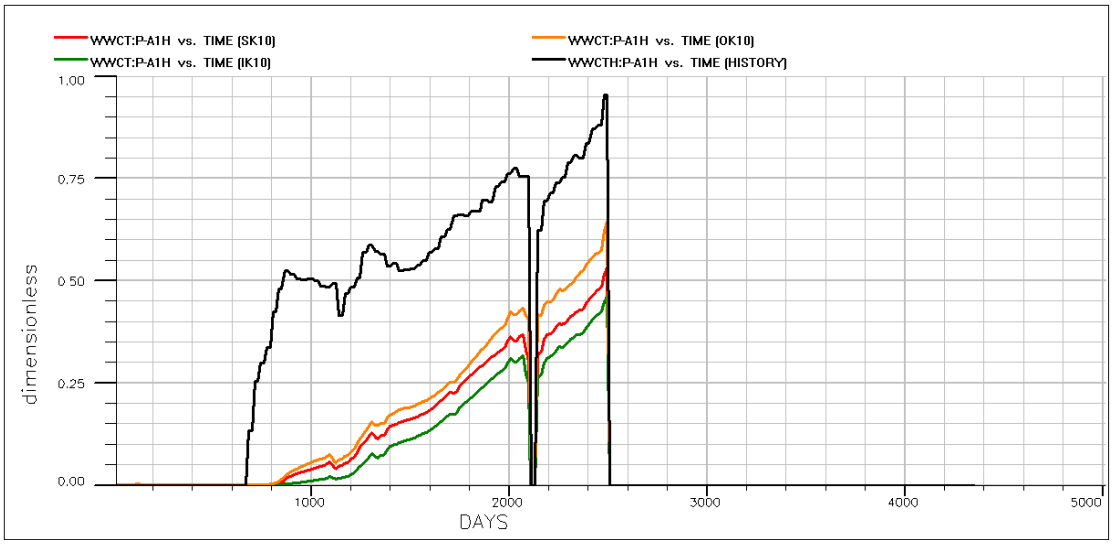

Figure 37 - Comparative chart of the predicted by the models IK10, OK10 and SK10 well water cut (WWCT) of P-A1H well with history data

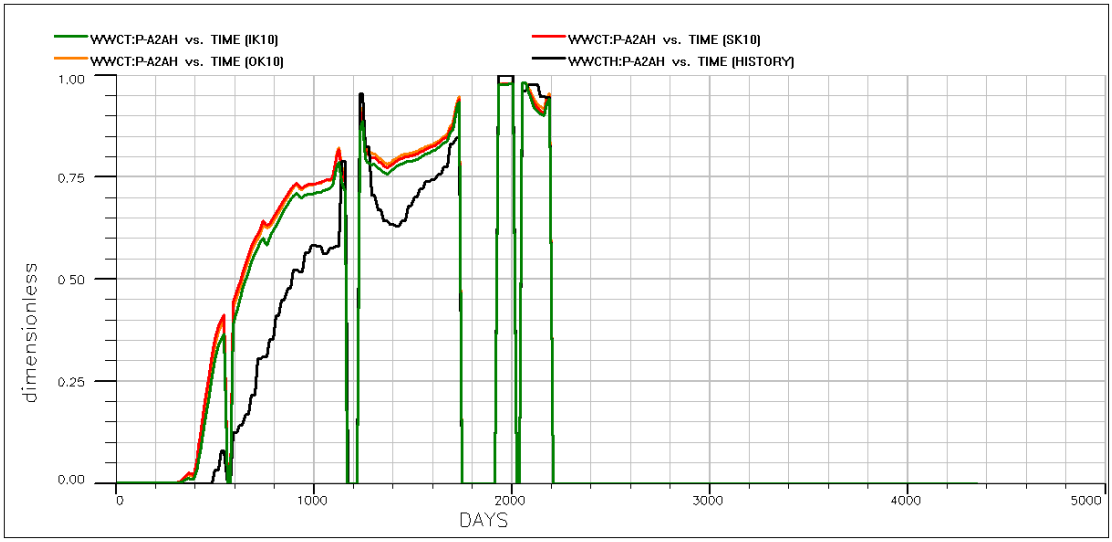

Figure 38 - Comparative chart of the predicted by the models IK10, OK10 and SK10 well water cut (WWCT) of P-A2AH well with history data

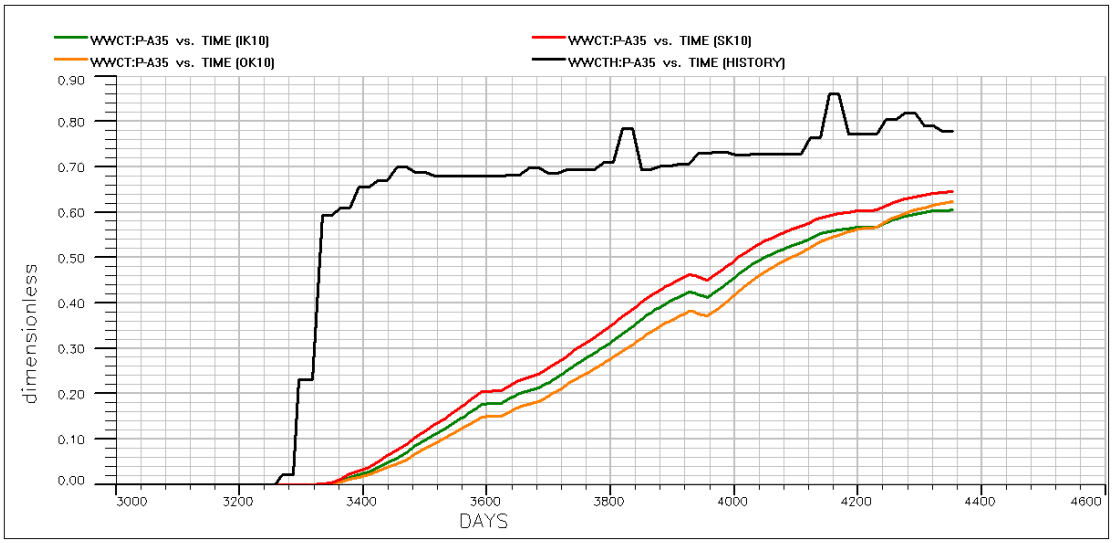

Figure 39 - Comparative chart of the predicted by the models IK10, OK10 and SK10 well water cut (WWCT) of P-A35 well with history data

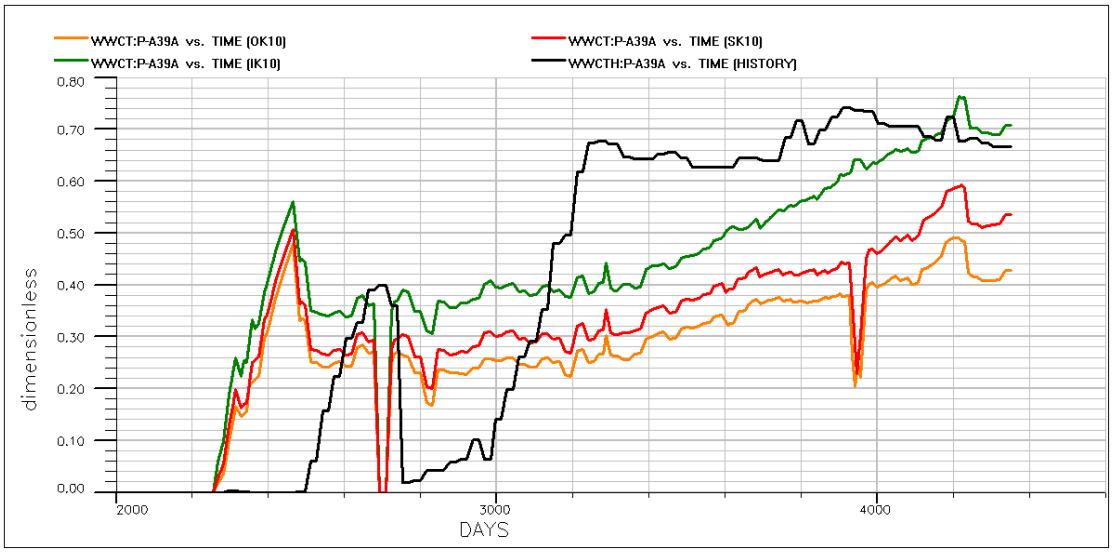

Figure 40 - Comparative chart of the predicted by the models IK10, OK10 and SK10 well water cut (WWCT) of P-A39A well with history data

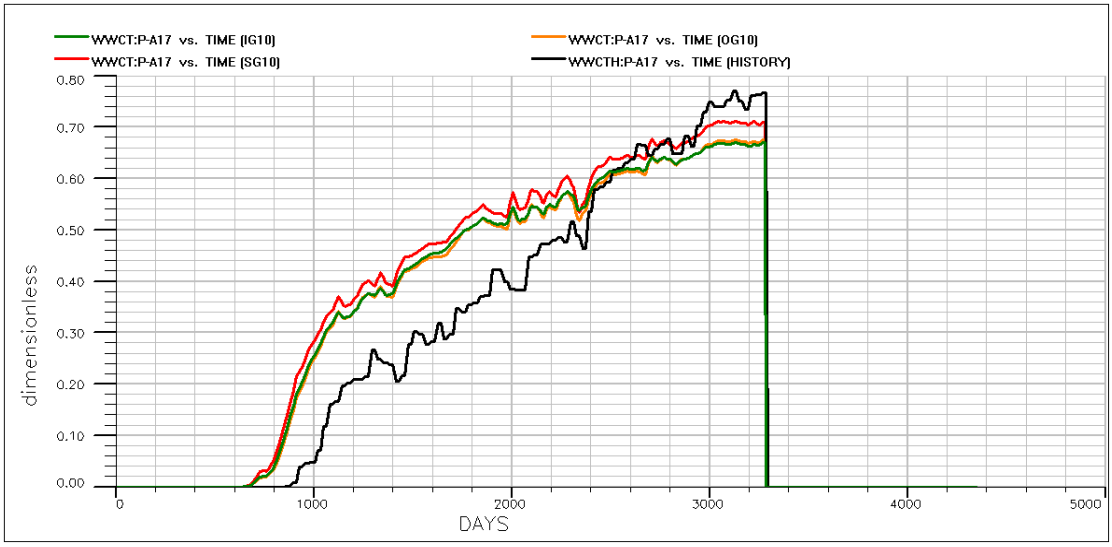

Figure 41 - Comparative chart of the predicted by the models IG10, OG10 and SG10 well water cut (WWCT) of P-A17 well with history data

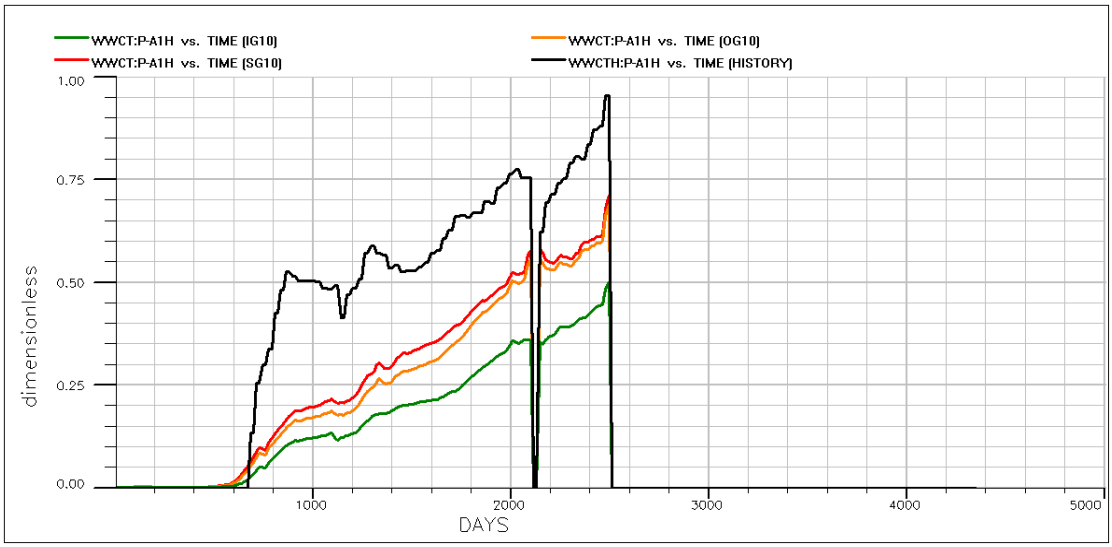

Figure 42 - Comparative chart of the predicted by the models IG10, OG10 and SG10 well water cut (WWCT) of P-A1H well with history data

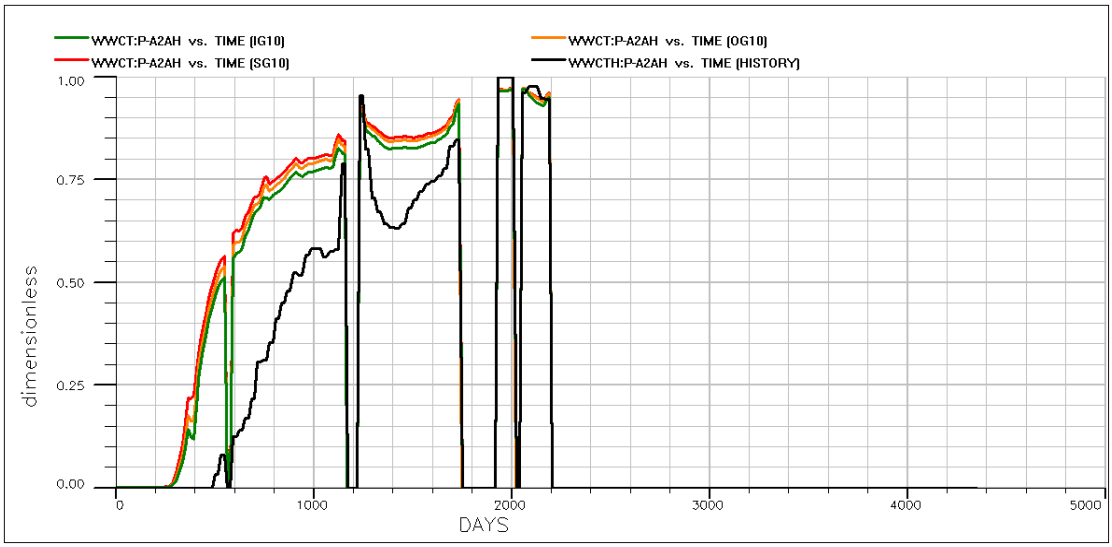

Figure 43 - Comparative chart of the predicted by the models IG10, OG10 and SG10 well water cut (WWCT) of P-A2AH well with history data

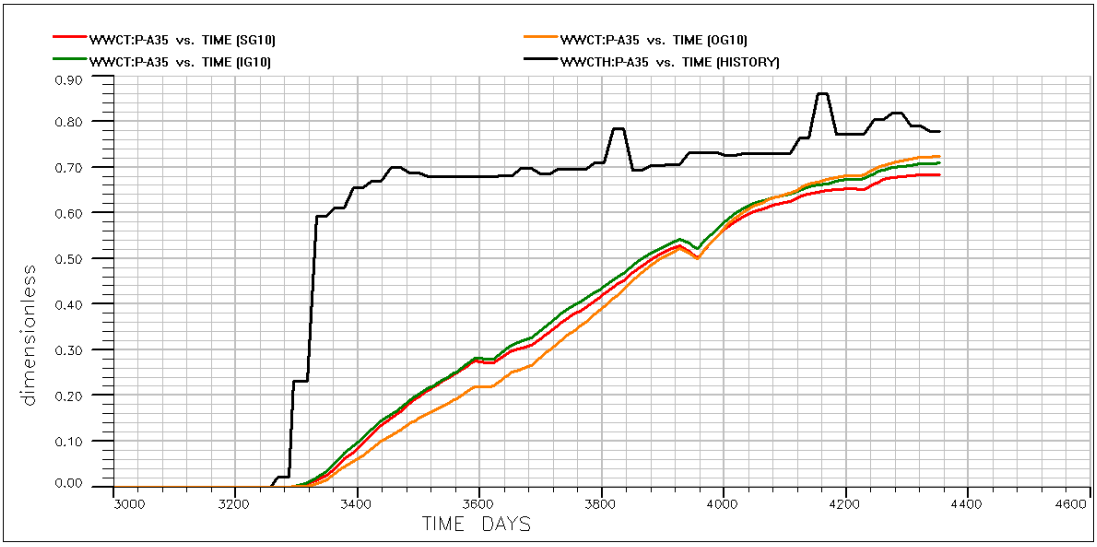

Figure 44 - Comparative chart of the predicted by the models IG10, OG10 and SG10 well water cut (WWCT) of P-A35 well with history data

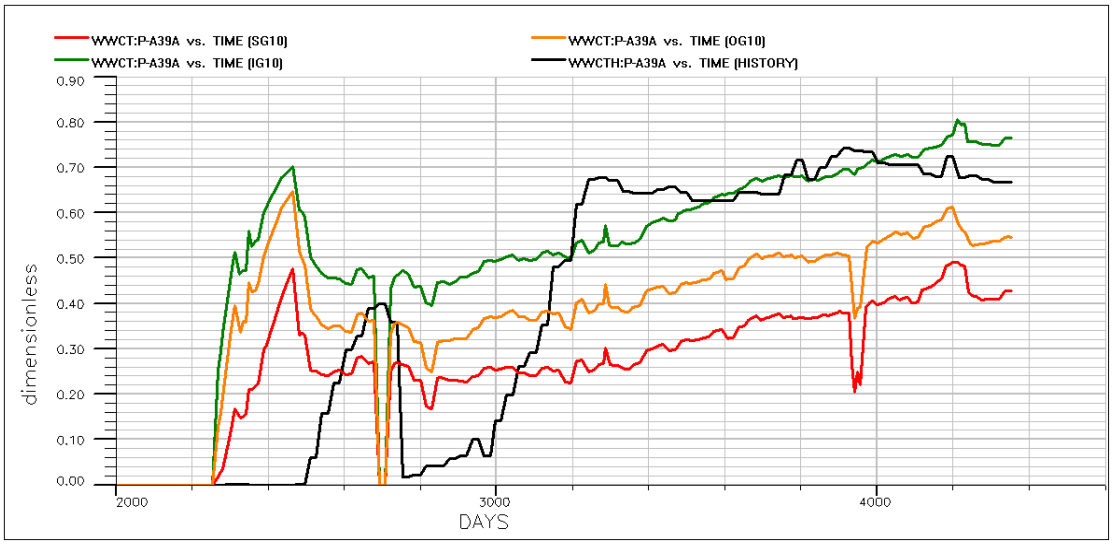

Figure 45 - Comparative chart of the predicted by the models IG10, OG10 and SG10 well water cut (WWCT) of P-A39A well with history data

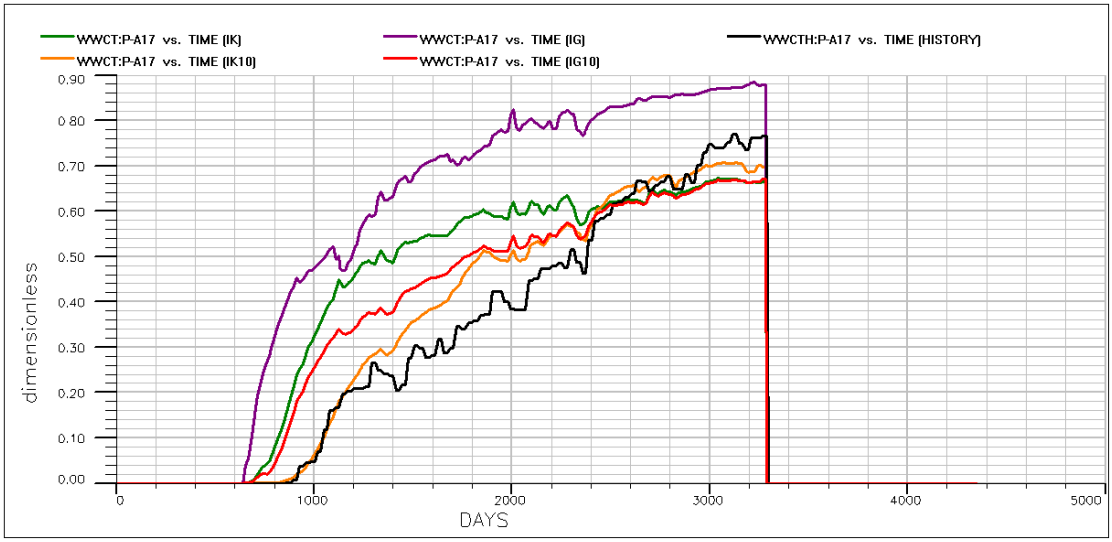

Figure 46 - Comparative chart of the predicted by the models IK, IK10, IG and IG10 well water cut (WWCT) of P-A17 with the history data

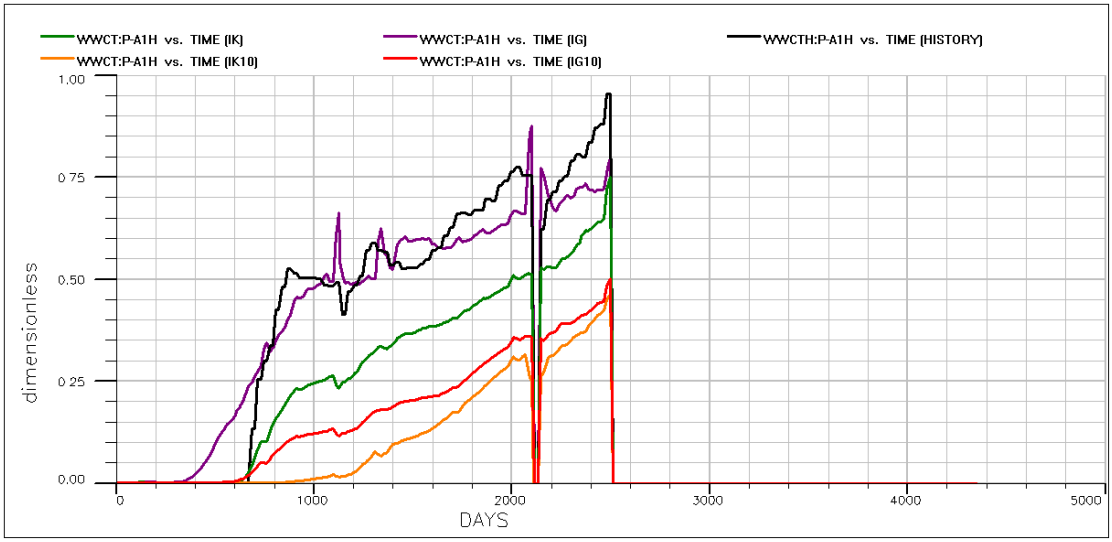

Figure 47 - Comparative chart of the predicted by the models IK, IK10, IG and IG10 well water cut (WWCT) of P- A1H with the history data

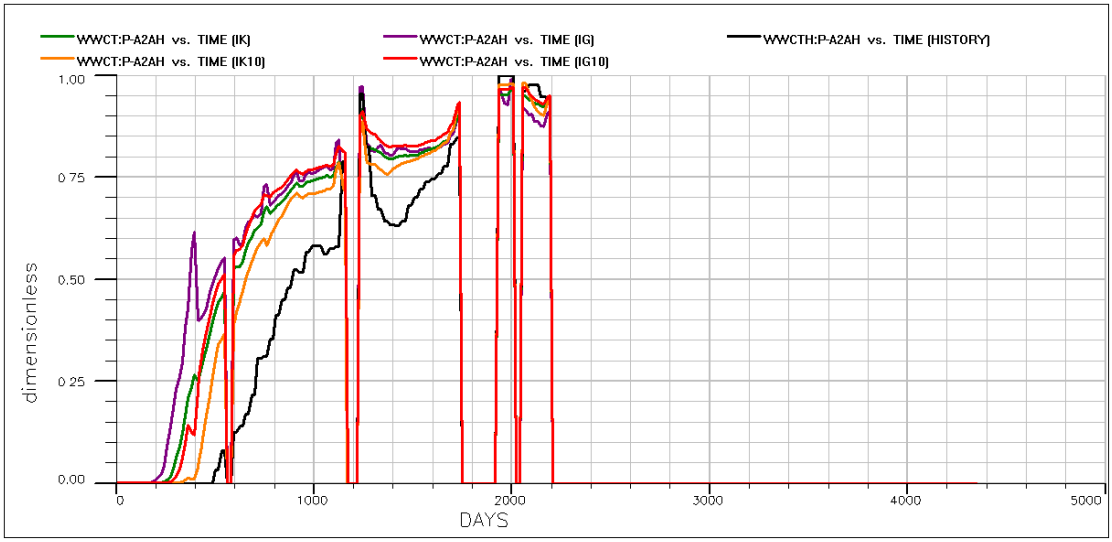

Figure 48 - Comparative chart of the predicted by the models IK, IK10, IG and IG10 well water cut (WWCT) of P- A2AH with the history data

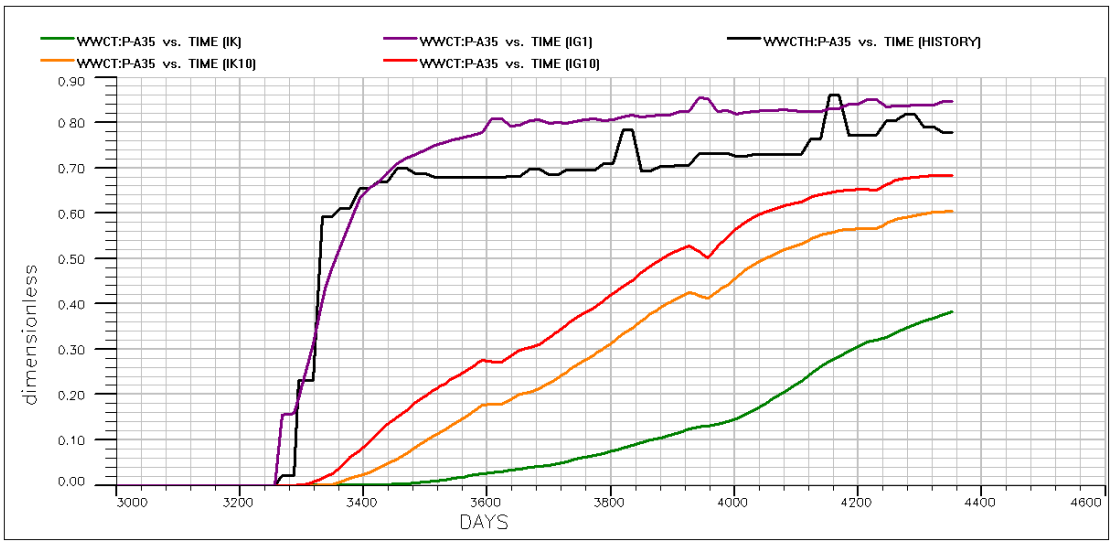

Figure 49 - Comparative chart of the predicted by the models IK, IK10, IG and IG10 well water cut (WWCT) of P-A35 with the history data

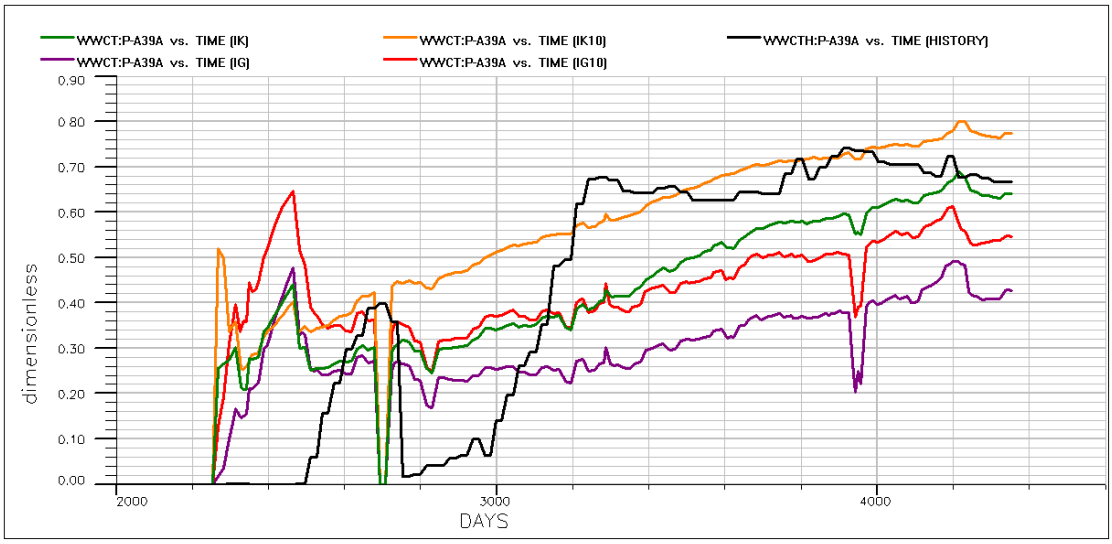

Figure 50 - Comparative chart of the predicted by the models IK, IK10, IG and IG10 well water cut (WWCT) of P-A39A with the history data

3.5.3 Comparison of the initial with the updated Dynamic model

Figure 51-55 present the well water predictions by the updated and the initial model which present differences between them. These differences are likely to reflect the impact of the updated structure has to the new dynamic model. Except this fact, it is considered based the seismic interpretation that the updated structure represents in a more consistent way the geological setting of the studied area.

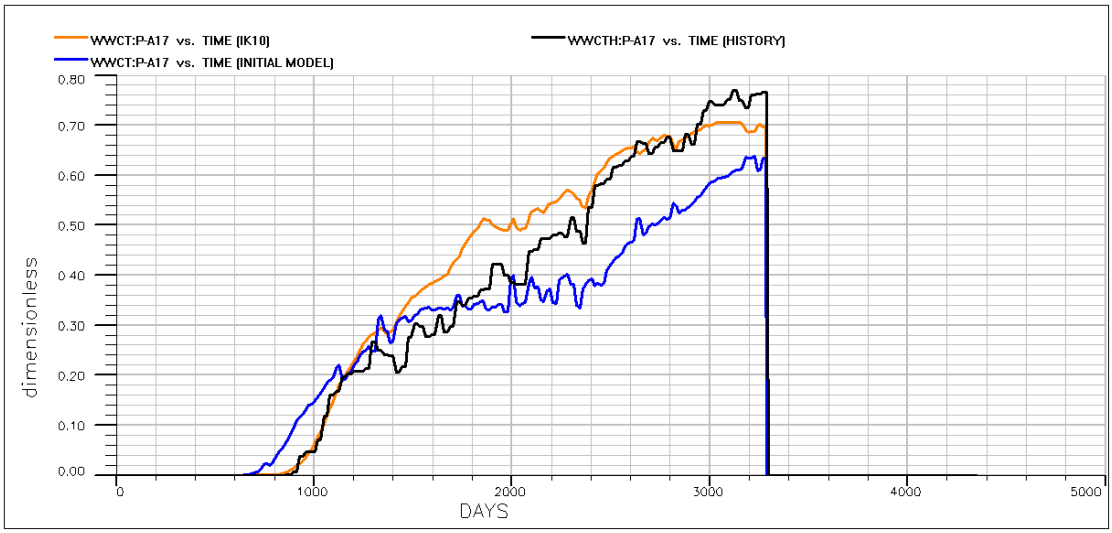

Figure 51 - Comparative chart of the predicted by the initial model and model IK10 well water cut (WWCT) of P-A17 with the history data

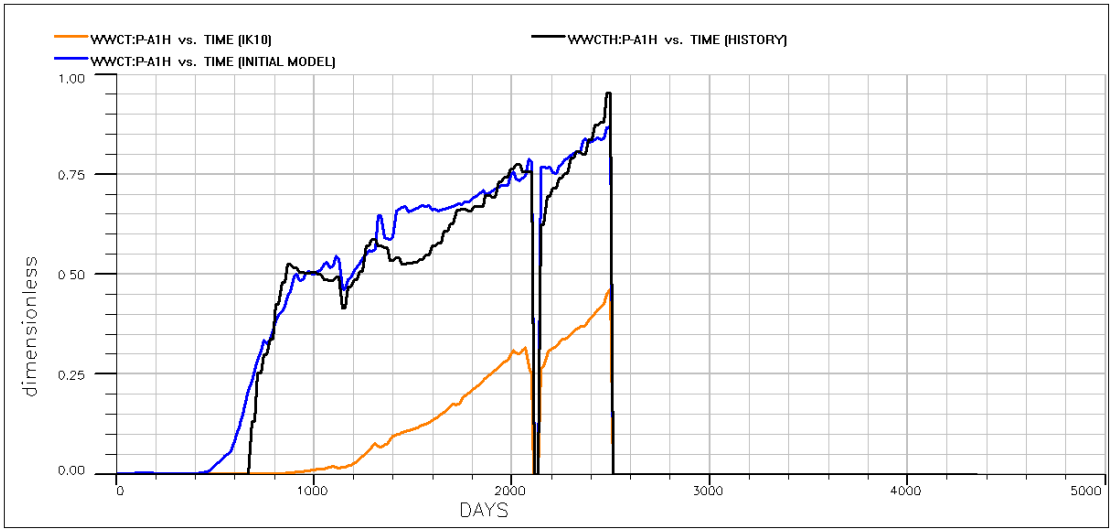

Figure 52 - Comparative chart of the predicted by the initial model and model IK10 well water cut (WWCT) of P-A1H with the history data

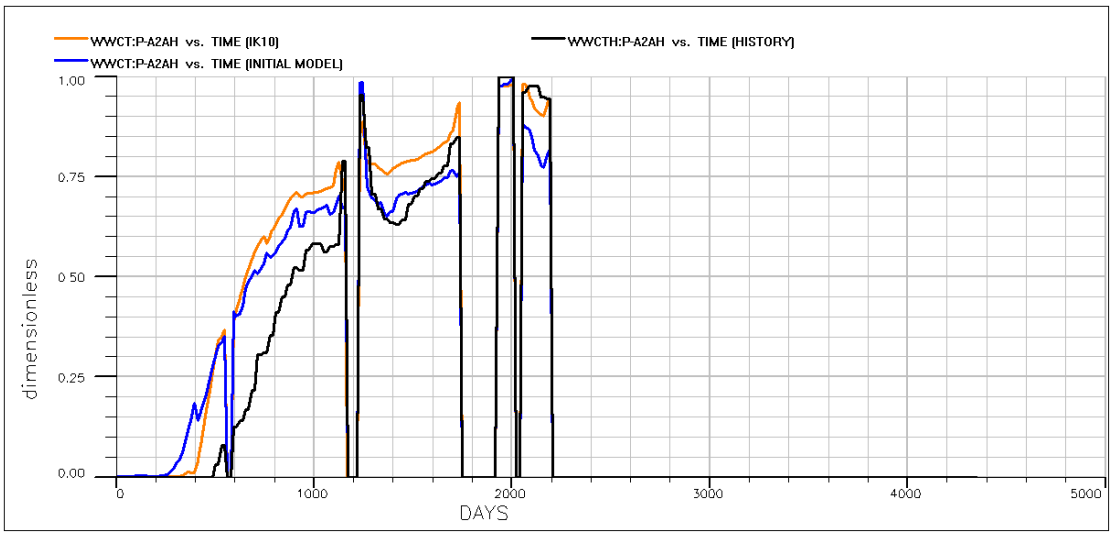

Figure 53 - Comparative chart of the predicted by the initial model and model IK10 well water cut (WWCT) of P-A2AH with the history data

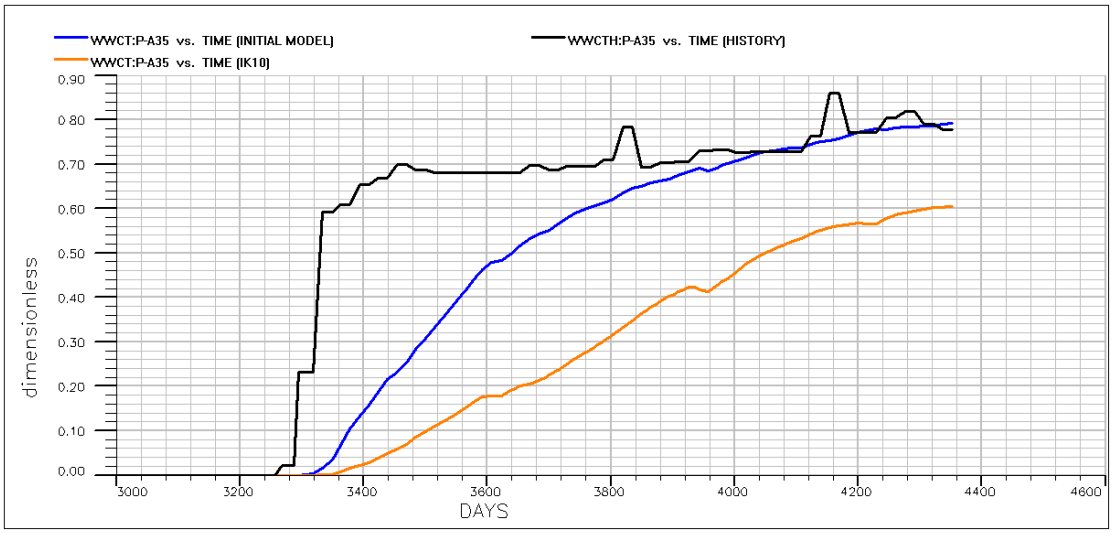

Figure 54 - Comparative chart of the predicted by the initial model and model IK10 well water cut (WWCT) of P-A35 with the history data

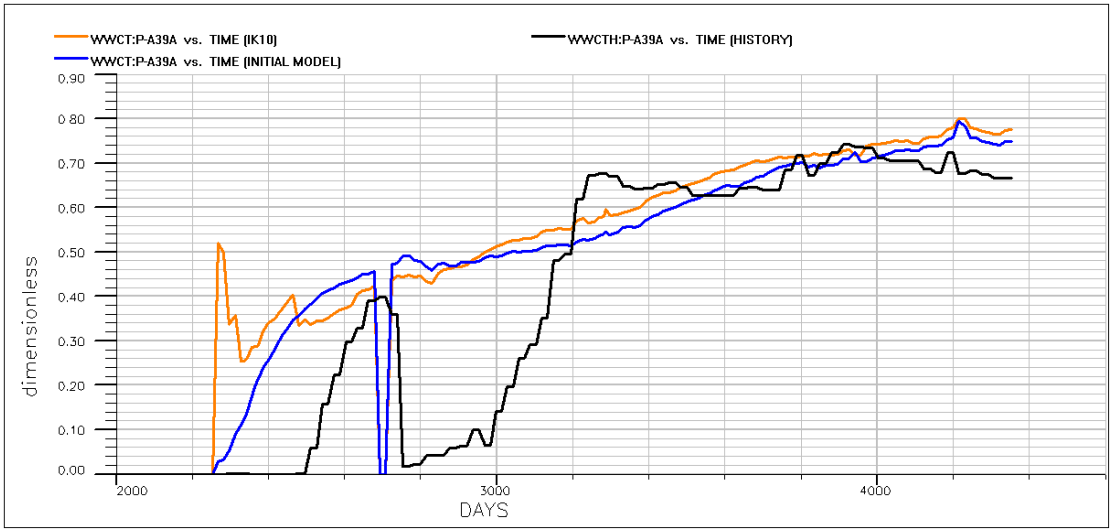

Figure 55 - Comparative chart of the predicted by the initial model and model IK10 well water cut (WWCT) of P-A39A with the history data

3.6 History matching

The final step was to match the prediction of the updated dynamic model with the history data. For the present thesis, the approach of history matching included the use of MULTX, MULTY and MULTZ in edit section. Using these commands, we can define a value which acts as an additional multiplier on the transmissibilities. A series of simulations performed by adjusting transmissibilities in order to match the updated model with history data.

The history matching procedure could be subdivided in two major groups of simulations. In the first one, the transmissibilities between all of the active grid cells were adjusted uniformly while in the second group of simulation adjustments performed in smaller areas. Helpful tools to this procedure were Eclipse office and Eclipse floviz.

Eclipse floviz is a visualization tool which can illustrate for the different time-steps of the simulation the dynamic properties of the model in a 3D environment. The monitoring of the oil or water saturations in certain section or layers through time was essential to the history match procedure (Figure 56). On the other hand, Eclipse office gives the ability for creating a variety of charts relevant of the simulation, like the ones used in the previous sections for demonstrating the well water cut. In such charts along the well water cut, the connection water cut was illustrated (Figure 57) giving the possibility to assess from which parts the wells produced more or less oil. In this way, valuable

information retread regarding the water propagation. Except this charts of total oil field production or total well production were used.

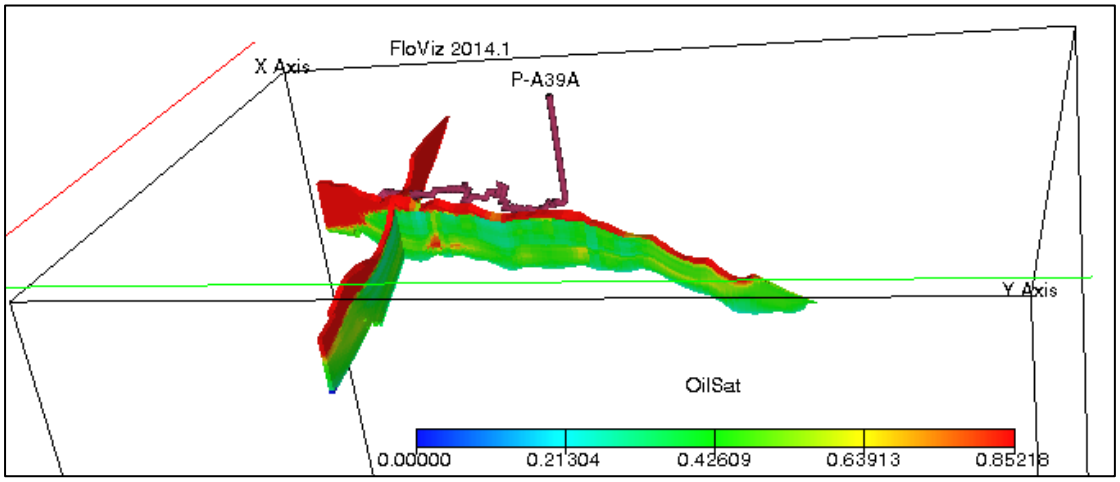

Figure 56 -Representation of oil saturation for slices i=55 and j=21 for model IK10G during the last step of simulation (01/10/1998) (z exaggeration=3)

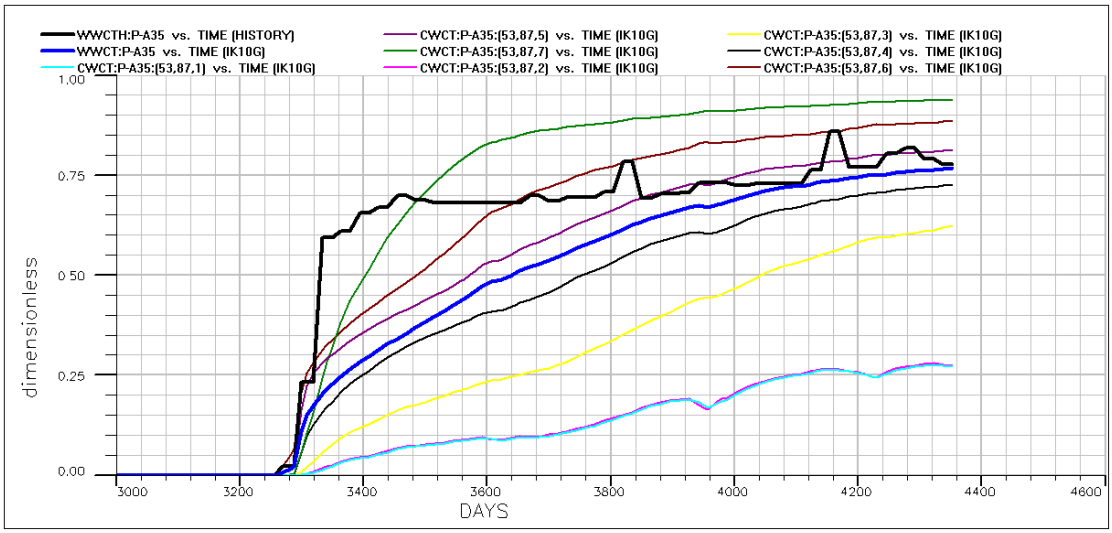

Figure 57 – An example of the charts used for history matching. The predicted by model IK10G well water cut along the connections water cut of well P-A35 with the history data

3.6.1 First group of simulations

The need a 'universal' adjustment in transmissibilities arise because the water propagation show a considerable lower speed moving on j direction than i and z directions. The resulting model out of this simulations group was IK10G. Figure 58 to 62 present comparative charts of the predicted well water cut (WWCT) by the models IK10 and IK10G model with the history data while Figure 63 to 64 present the predicted by these models field water cut (FWCT) and total oil field production (FOPT) with history data. The previous charts clearly represent the improvement of the predictions of the updated dynamic model IK10G. The final values of MULT-X, -Y and -Z is 0.5, 2 and 0.25 respectively.

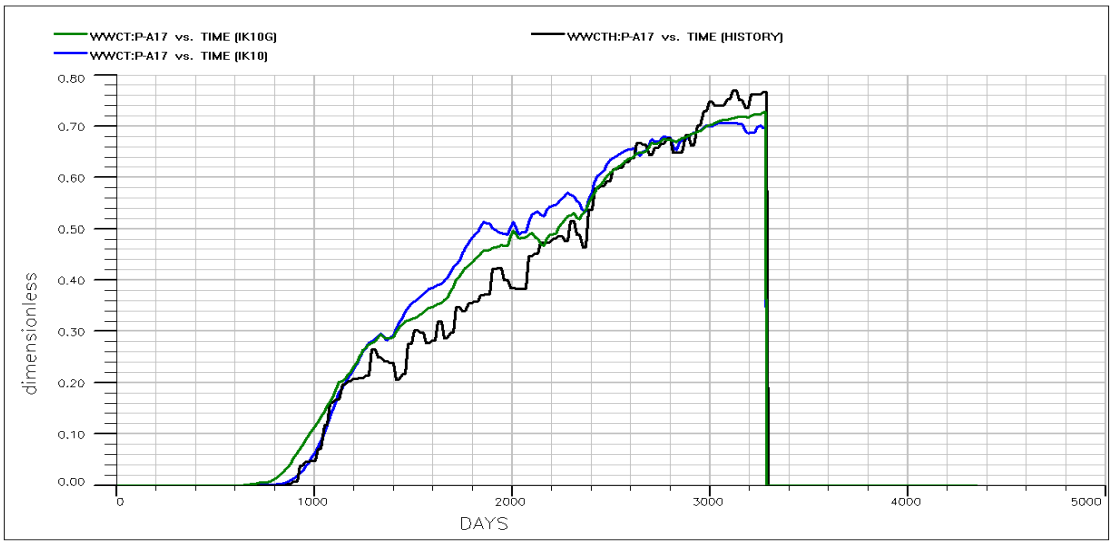

Figure 58 – Comparitive chart of the predicted well water cut of P-A17 by the model IK10 and IK10G with the history data

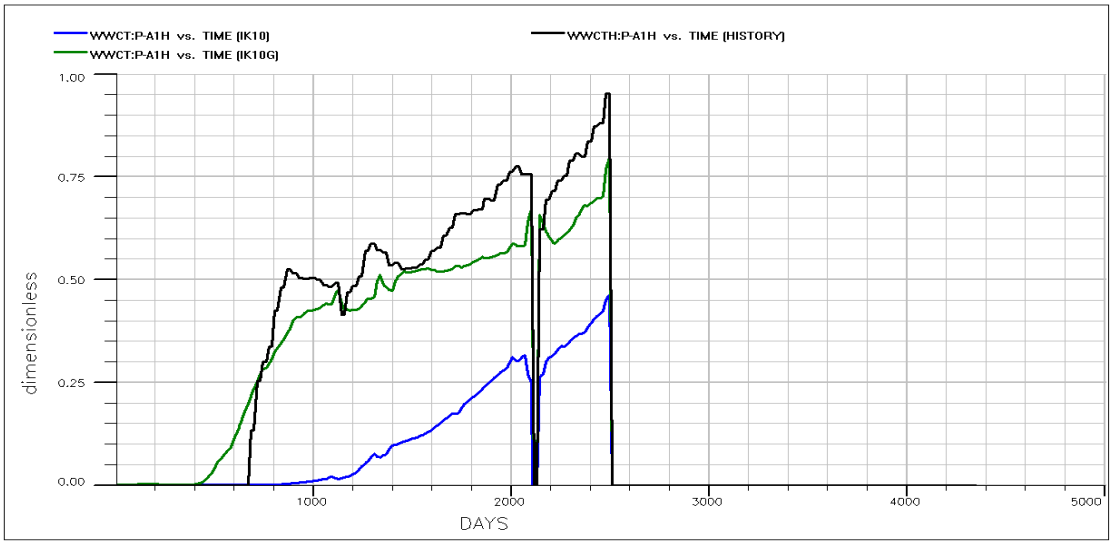

Figure 59 – Comparitive chart of the predicted well water cut of P-A1H by the model IK10 and IK10G with the history data

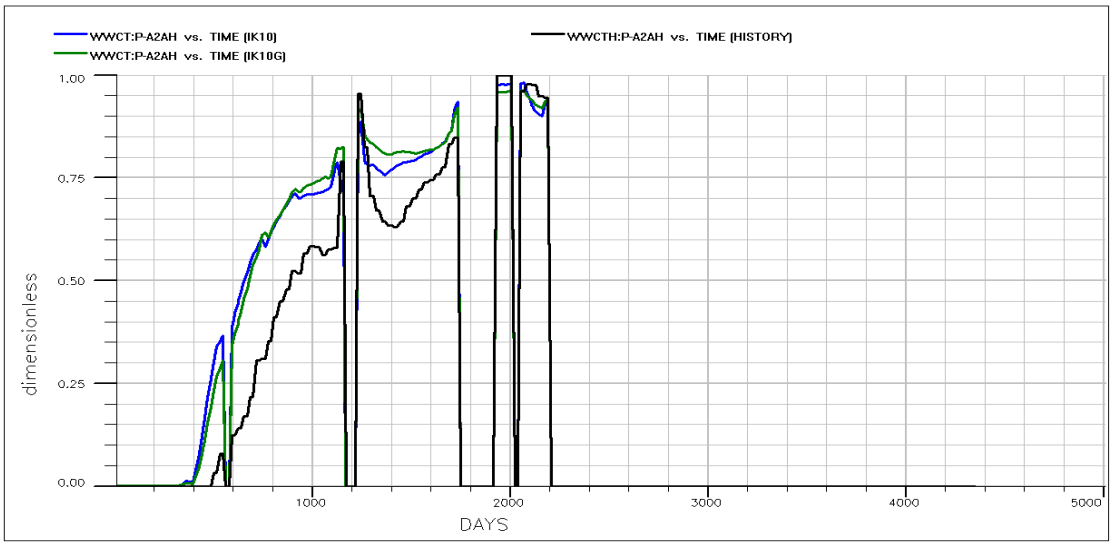

Figure 60 - Comparitive chart of the predicted well water cut of P-A2AH by the model IK10 and IK10G with the history data

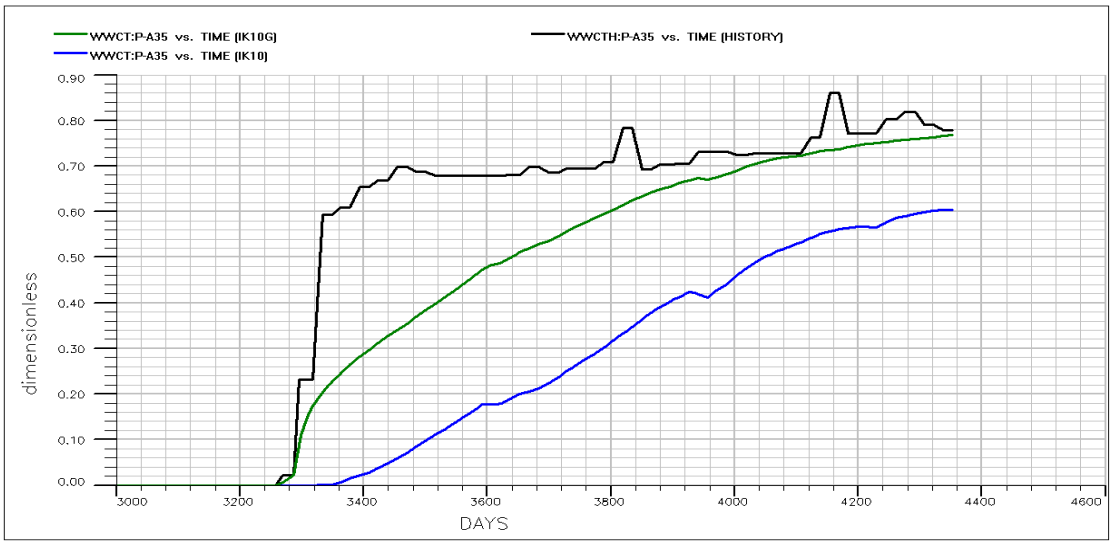

Figure 61 – Comparitive chart of the predicted well water cut of P-A35 by the model IK10 and IK10G with the history data

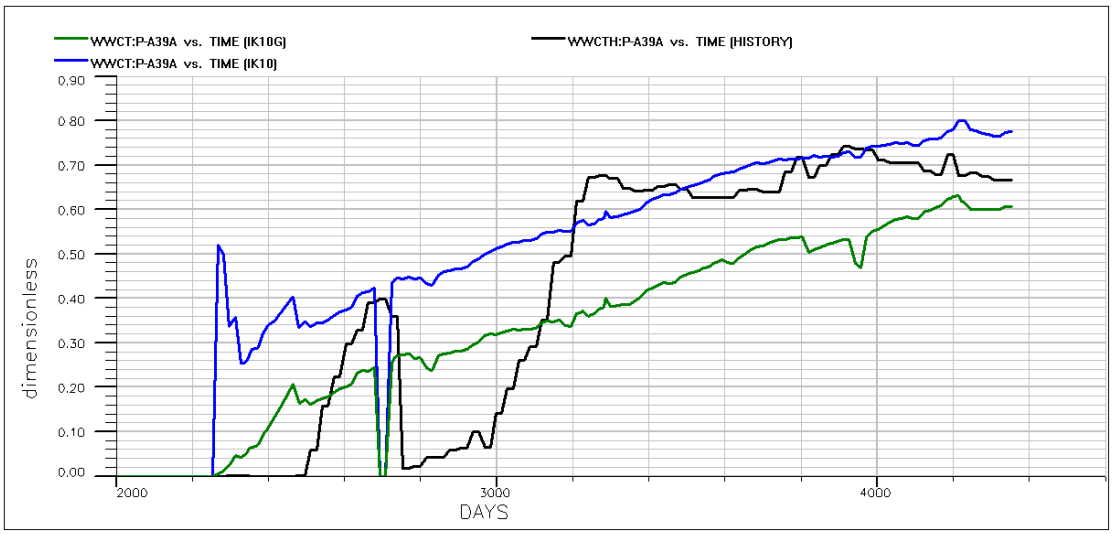

Figure 62 - Comparitive chart of the predicted well water cut of P-A39A by the model IK10 and IK10G with the history data

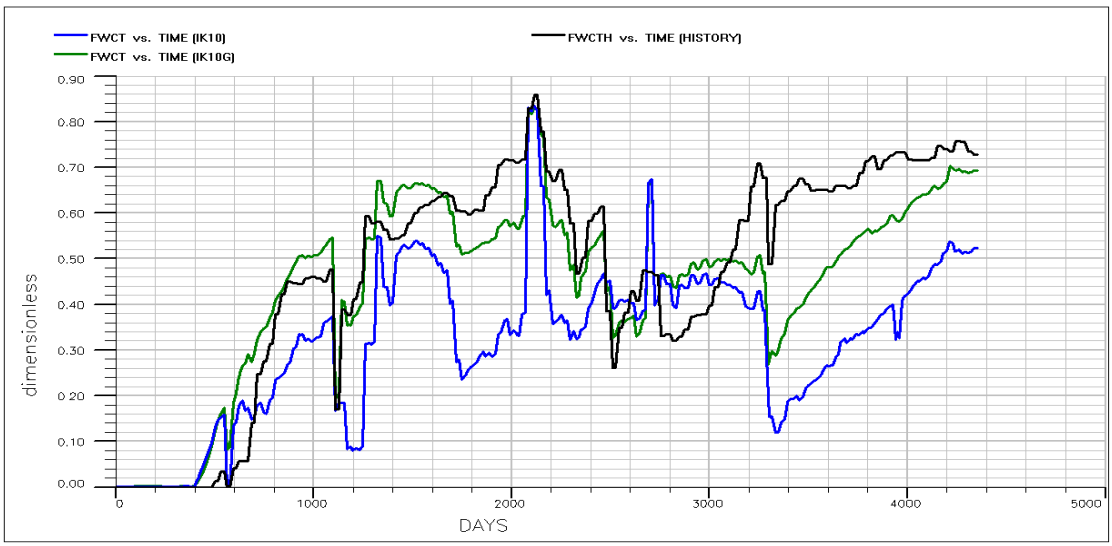

Figure 63 - Comparitive chart of the predicted field water cut (FWCT) by the model IK10 and IK10G with history data

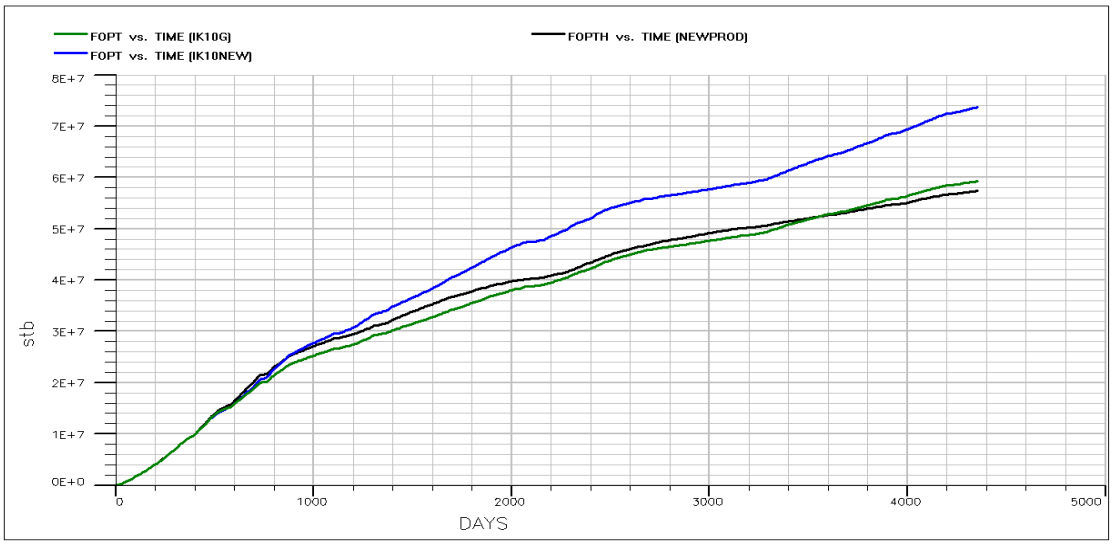

Figure 64 - Comparitive chart of the predicted total oil field production (FOPT) by the model IK10 and IK10G with history data

3.6.2 Second group of simulations

After the rough tuning of the model in the first simulations group, now the transmissibilities were adjusted in smaller areas keeping at the same time the previous transmissibilities changes.

The resulted model was model A25 which is the history matched model. Figure 65 to 69 present the improvement of the well water cut predictions of the model A25 against model IK10G.

Figure 70 and Figure 71 illustrate the final prediction of total oil field production and field water cut between model A25 model with the history data. The simulation boxes with the transmissibility multipliers used for the second simulations group are presented in APPENDIX APPENDIX .

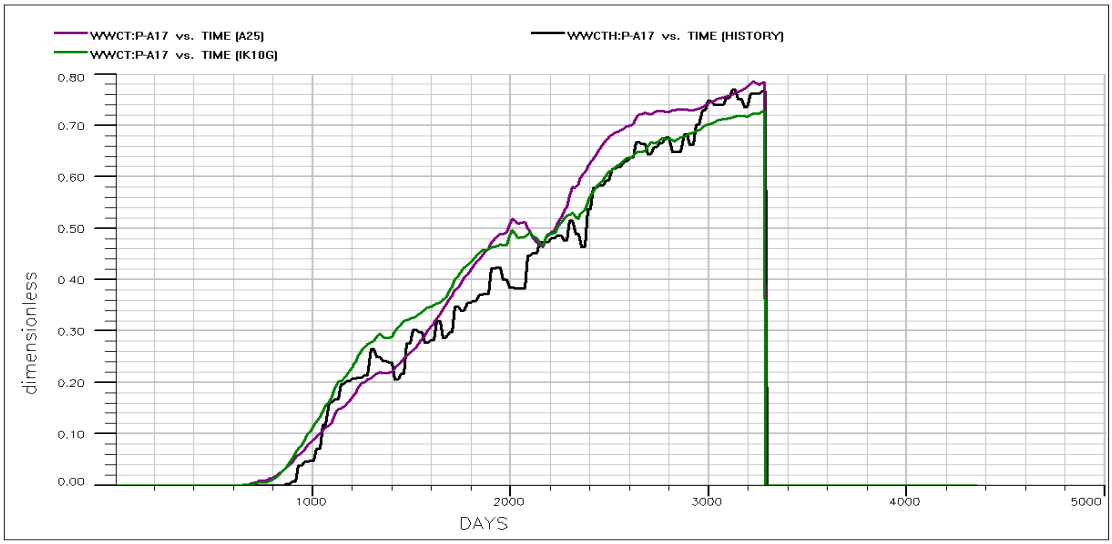

Figure 65 - Comparitive chart of the predicted well water cut of P-A17 by the model IK10G and A25 with the history data

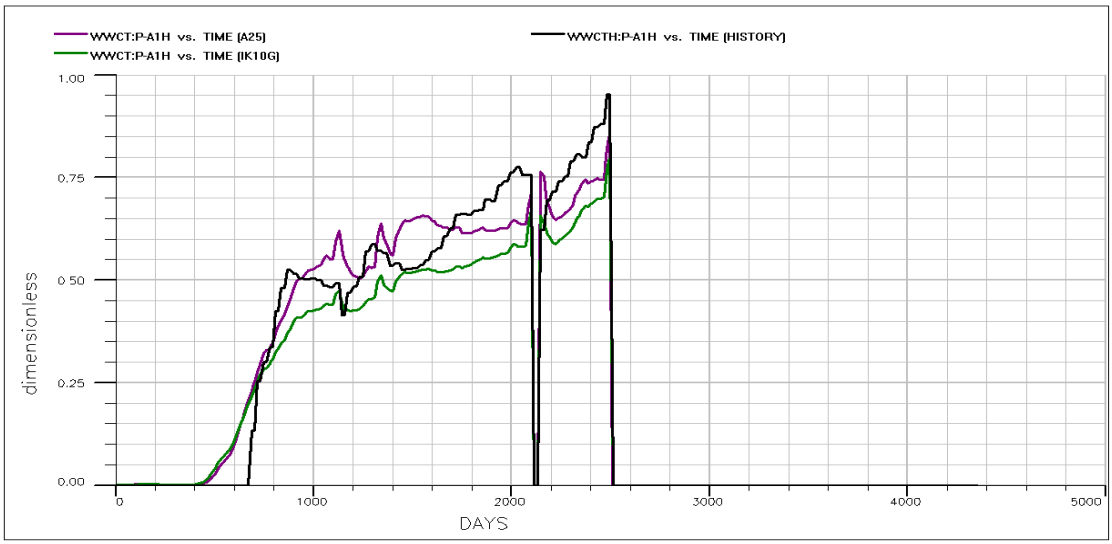

Figure 66 – Comparitive chart of the predicted well water cut of P-A1H by the model IK10G and A25 with the history data

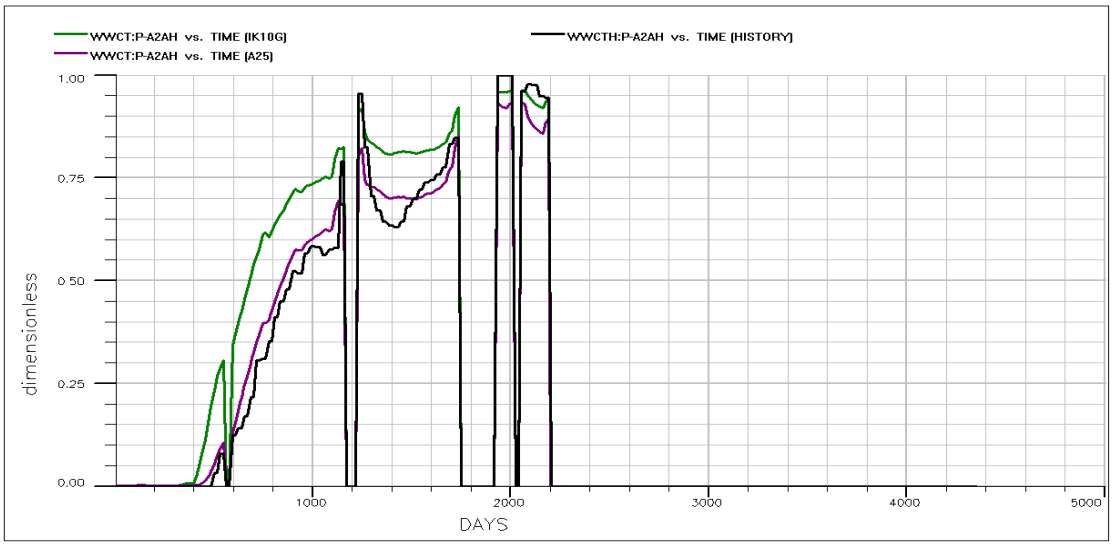

Figure 67 - Comparitive chart of the predicted well water cut of P-A2AH by the model IK10G and A25 with the history data

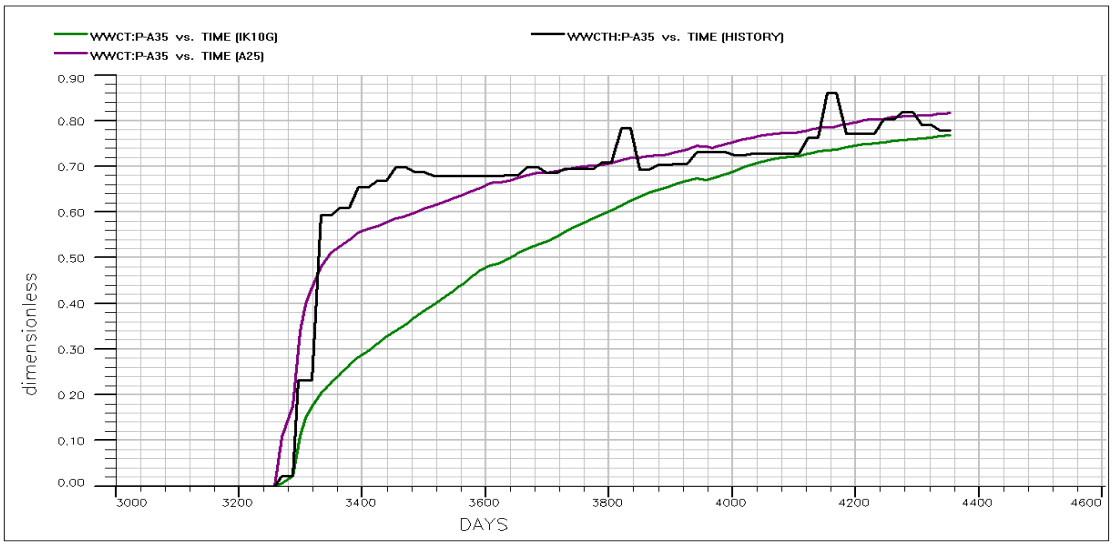

Figure 68 - Comparitive chart of the predicted well water cut of P-A35 by the model IK10G and A25 with the history data

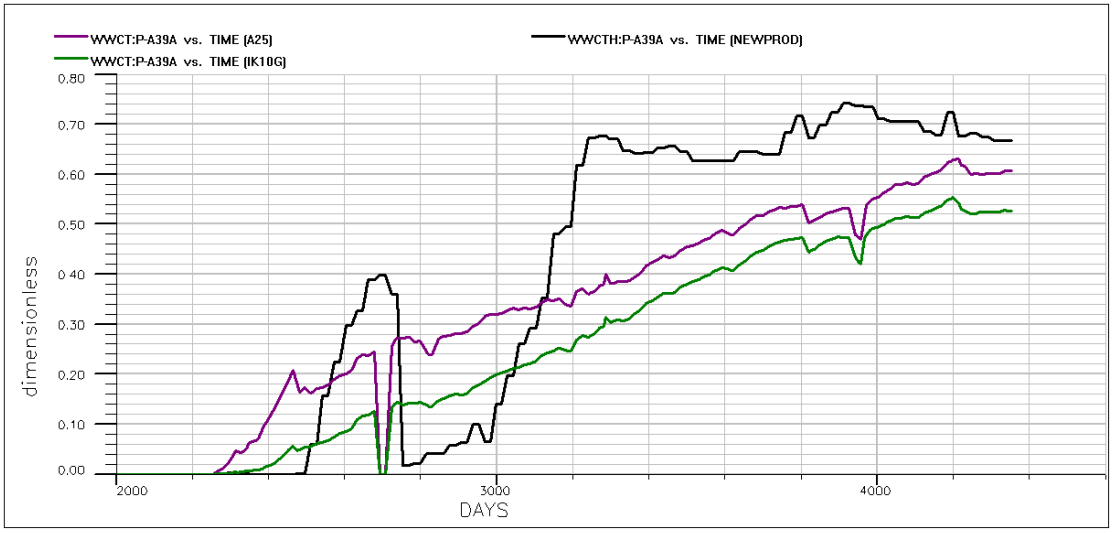

Figure 69 - Comparitive chart of the predicted well water cut of P-A39A by the model IK10G and A25 with the history data

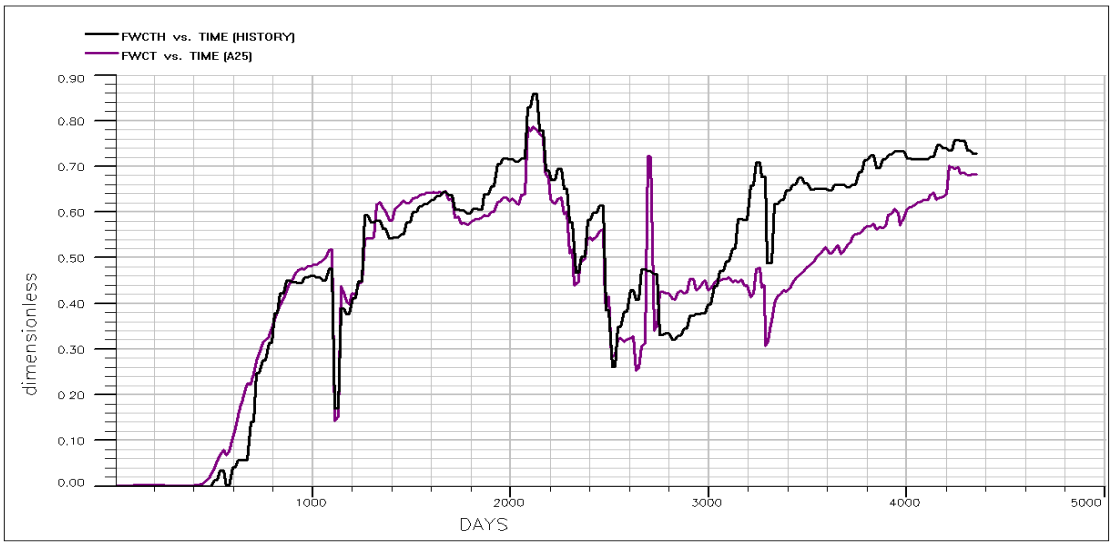

Figure 70 - Compartive chart of field water cut (FWCT) of the hisory matched model (A25) with history data

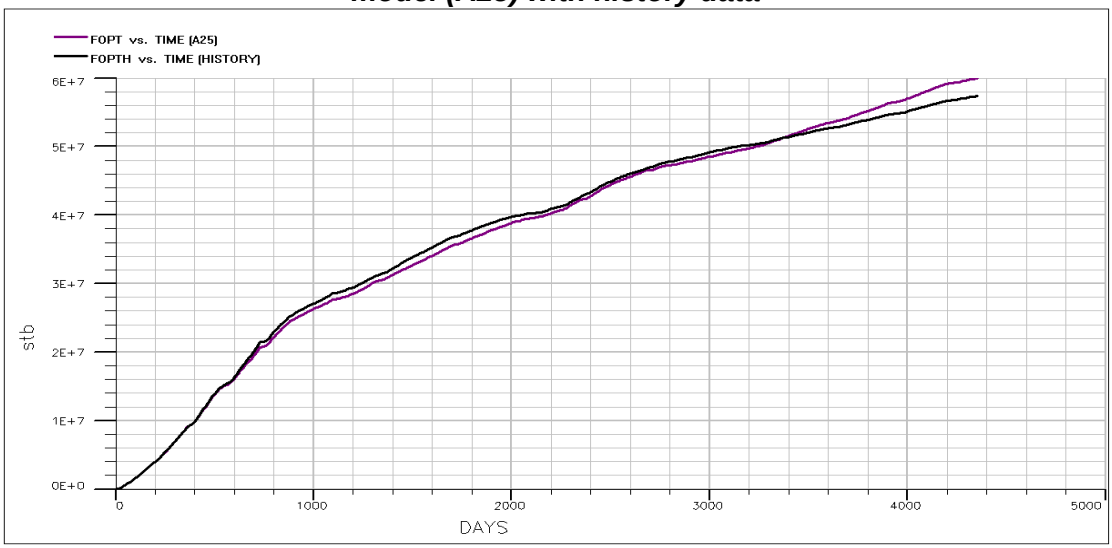

Figure 71 – Compartive chart of total oil field production (FOPT) of the hisory matched model (A25) with history data

4 Conclusion

In the context of this thesis, the combination of two different datasets resulted in:

- Re-interpretation of faults and Top- and Base-structure of Lower Brent Group based on a new seismic dataset
- Construction of 12 static models which
- Construct as many dynamic models
- Assessment of the efficiency of the constructed dynamic models

Finally, a new dynamic model for H1 segment constructed. The model was tuned by modifying transmissibilities in order to produce predictions as close to the history production data.

The predictions of the new dynamic model were different compared to those of the initial dynamic model, which most probably reflect the impact the updated structure has. However, based on the interpretation of the available seismic data it is considered that the updated structure is more consistent to geological setting of the area that the seismic reveal. Thus, by having a more representative geological static model and the production data history matched on the new grid, we then consider that the updated dynamic model can predict the future performance of the studied reservoir with more confidence.

REFFERENCES

Alveberg, L-J., & Melberg, E.V. (2013). Fact 2013. The Norwegian petroleum sector. Ministry of Petroleum and Energy.

Folkestad, A., Odinsen, T., Fossen, H., & Pearce, M. A. (2014). Tectonic influence on the Jurassic sedimentary architecture in the northern North Sea with focus on the Brent Group. *From Depositional Systems to Sedimentary Successions on the Norwegian Continental Margin*, 389–415. http://doi.org/10.1002/9781118920435.ch14

Fossen, H. (1989). Indication of transpressional tectonics in the Gullfaks oil-field, northern North Sea. *Marine and Petroleum Geology*, *6*(1). http://doi.org/10.1016/0264-8172(89)90073-1

Fossen, H., & Hesthammer, J. (1998). Structural geology of the Gullfaks Field, northern North Sea. (1998). In: Coward, M. P., Daltaban, T. S.,Johnson, H. (eds) Structural geology in reservoir characterization. Geological Society, London, Special Publications, 127, 231–261

Fossen, H., & Hesthammer, J. (2000). Possible absence of small faults in the Gullfaks Field, northern North Sea: Implications for downscaling of faults in some porous sandstones. *Journal of Structural Geology*, *22*(7), 851–863. http://doi.org/10.1016/S0191-8141(00)00013-4

Fossen, H., & Rørnes, A. (1996). Properties of fault populations in the Gullfaks Field, northern North Sea. *Journal of Structural Geology*, *18*(2–3), 179–190. http://doi.org/10.1016/S0191-8141(96)80043-5

Hesthammer, J., & Fossen, H. (2001). Structural core analysis from the Gullfaks area, northern North Sea. *Marine and Petroleum Geology*, *18*(3), 411–439. http://doi.org/10.1016/S0264-8172(00)00068-4

Hesthammer, J., & Fossen, H. (1999). Evolution and geometries of gravitational collapse structures with examples from the Statfjord Field, northern North Sea. *Marine and Petroleum Geology*, *16*(3), 259–281. http://doi.org/10.1016/S0264-8172(98)00071-3

Gullfaks Reservoir Management Plan (Gullfaks RMP). (2007). Reservoarstyringsplan 2007 for Gullfaks. StatoilHydro.

Rouby, D., Fossen, H., & Cobbold, P. R. (1996). Extension , Displacement , and Block Rotation in the from Map View Restoration 1 Gullfaks-Statfjord area. *American Association of Petroleum Geologists Bulletin*, *6*(6), 875–890. http://doi.org/10.1306/64ED88F4-1724-11D7-8645000102C1865D

Rivenæs, J., Sørhaug P., C., & Knarud, R., (2010) Introduction to reservoir modelling. In *Petroleum Geoscience*. Ed: Bjorlykke, K.,. http://doi.org/10.1007/978-3-642-02332-3

Siddiqui, N. A., Mathew, M. J., Menier, D., & Hassaan, M. (2016). 2D and 3D seismic simulation for fault modeling: exploratory revision from the Gullfaks field. *Journal of Petroleum Exploration and Production Technology*. http://doi.org/10.1007/s13202-016-0301-3

Spencer, A. M., Briskeby, P. I., Christensen, L. D., Foyn, R., Kjølleberg, M., Kvadsheim, E., … Williams, J. (2008). Petroleum geoscience in Norden – Exploration, production and organization. *Episodes*, *31*(1), 115–124.

Talukdar, S., & Instefjord, R. (2008). SPE 113260 Reservoir Management of the Gullfaks Main Field. *Group*, (June 2008), 9–12. Retrieved from

Tollefsen, S., Graue, E., Svinddal, S., & Ais, S. (1992). SPE 25054.

Yielding, G., Overland, J. A., & Byberg, G., (1999) Characterization of fault zones for reservoir modelling: an example from the Gullfaks Field, northern North Sea. Bull AAPG 83:925–951

APPENDIX

Table 5 - Description of the boxes used in the second group of simulation in edit section. Along this box MULTX=0.5, MULTY=2 and MULTZ=0.25 for i=1 to 78, j=1 to 131 and z=1 to 37 (first simulations group)

Model	Keyword	Value	i1	i2	j1	j2	k1	k2
A1	MULTZ	0.01	38	78	72	131	16	37
A2	MULTZ	10	48	65	72	131	16	37
A3	MULTY	0.5	38	78	79	131	13	37
A4	MULTY	0.5	38	78	79	131	13	37
A5	MULTY	0.5	38	78	79	131	13	37
A6	MULTY	0.5	38	78	79	131	13	37
	MULTZ	10	38	78	79	131	13	37
A7	MULTY	0.001	38	78	79	131	13	37
	MULTZ	10	38	78	79	131	13	37
A8	MULTX	0.1	40	50	23	65	1	37
	MULTY	0.001	38	78	79	131	13	37
	MULTZ	10	38	78	79	131	13	37
A9	MULTX	0.2	40	55	23	75	1	37
	MULTY	0.001	38	78	79	131	13	37
	MULTZ	10	38	78	79	131	13	37
A10	MULTX	0.2	40	55	23	75	1	37
	MULTY	0.001	38	78	79	131	13	37
	MULTY	5	33	78	53	78	1	37
	MULTZ	10	38	78	79	131	13	37
A11	MULTX	0.2	40	55	23	56	1	37
	MULTY	0.001	38	78	79	131	13	37
	MULTY	5	33	78	53	78	1	37
	MULTZ	10	38	78	79	131	13	37
A12	MULTX	0.2	40	55	23	56	1	37
	MULTX	0.3	40	55	57	75	1	37
	MULTY	0.001	38	78	79	131	13	37
	MULTY	5	33	78	53	78	1	37
	MULTZ	10	38	78	79	131	13	37
A13	MULTX	0.2	40	55	23	56	1	37
	MULTX	0.35	40	55	57	75	1	37
	MULTY	0.001	38	78	79	131	13	37
	MULTY	5	33	78	53	78	1	37
	MULTZ	0.001	37	53	13	28	16	16
	MULTZ	10	38	78	79	131	13	37
A14	MULTX	0.2	40	55	23	56	1	37
	MULTX	0.35	40	55	57	75	1	37
	MULTY	0.001	38	78	79	131	13	37
	MULTY	5	33	78	53	78	1	37
	MULTZ	0.001	37	53	13	28	16	16
	MULTZ	0.001	47	53	13	28	14	14
	MULTZ	10	38	78	79	131	13	37
A15	MULTX	0.2	40	55	23	56	1	37
	MULTX	0.35	40	55	57	75	1	37
	MULTY	0.001	38	78	79	131	13	37
	MULTY	5	33	78	53	78	1	37
	MULTZ	0.001	37	78	13	28	16	16
	MULTZ	0.001	47	78	13	28	14	14
	MULTZ	10	38	78	79	131	13	37
A16	MULTX	0.2	40	55	23	56	1	37
	MULTX	0.35	40	55	57	75	1	37
	MULTY	0.001	38	78	79	131	13	37
	MULTY	5	33	78	53	78	1	37
	MULTZ	0.001	37	78	13	40	16	16
	MULTZ	0.001	47	78	13	40	14	14
	MULTZ	10	38	78	79	131	13	37
A17	MULTX	0.2	40	55	23	56	1	37
	MULTX	0.35	40	55	57	75	1	37
	MULTY	0.001	38	78	79	131	13	37
	MULTY	5	33	78	53	78	1	37
	MULTZ	0.001	37	78	13	40	16	16
	MULTZ	0.001	47	78	13	40	14	14
	MULTZ	10	38	78	79	131	13	37
	MULTZ	0.001	13	53	12	42	9	9
A18	MULTX	0.2	40	55	23	56	1	37
	MULTX	1E-06	13	13	31	50	1	9
	MULTX	0.35	40	55	57	75	1	37
	MULTY	0.001	38	78	79	131	13	37
	MULTY	5	33	78	53	78	1	37
	MULTZ	0.001	37	78	13	40	16	16
	MULTZ	0.001	47	78	13	40	14	14
	MULTZ	10	38	78	79	131	13	37
	MULTZ	0.001	13	53	12	42	9	9
A19	MULTX	0.2	40	55	23	56	1	37
	MULTX	1E-06	13	13	31	50	1	9
	MULTX	0.35	40	55	57	75	1	37
	MULTY	0.001	38	78	79	131	13	37
	MULTY	0.5	1	18	18	38	1	16
	MULTY	5	33	78	53	78	1	37
	MULTZ	0.001	47	78	13	40	14	14
	MULTZ	10	38	78	79	131	13	37
	MULTZ	0.001	13	53	12	42	9	9
A20	MULTX	0.2	40	55	23	56	1	37

A21	MULTY	1E-06	13	13	31	50	1	21
	MULTX	0.3	40	55	57	75	1	37
	MULTY	0.001	38	78	79	131	13	37
	MULTY	0.5	1	18	18	38	1	16
	MULTY	5	33	78	53	78	1	37
	MULTZ	0.001	37	78	13	40	16	16
	MULTZ	0.001	47	78	13	40	14	14
	MULTZ	10	38	78	79	131	13	37
	MULTZ	0.001	13	53	12	42	9	9
A22	MULTX	0.2	40	55	23	56	1	37
	MULTX	0.3	40	55	57	75	1	37
	MULTY	0.001	38	78	79	131	13	37
	MULTY	0.5	1	18	18	38	1	16
	MULTY	5	33	78	53	78	1	37
	MULTZ	0.001	37	78	13	50	16	16
	MULTZ	0.001	37	78	13	50	14	14
	MULTZ	10	38	78	79	131	13	37
	MULTZ	0.001	13	53	12	42	9	9
A23	MULTX	0.2	40	55	23	56	1	37
	MULTX	1E-06	13	13	31	50	1	9
	MULTX	0.35	40	55	57	75	1	37
	MULTY	0.001	38	78	79	131	13	37
	MULTY	0.5	1	18	18	38	1	16
	MULTY	5	33	78	53	78	1	37
	MULTZ	0.001	37	78	13	40	16	16
	MULTZ	0.001	47	78	13	40	14	14
	MULTZ	10	38	78	79	131	13	37
	MULTZ	0.001	13	53	12	42	9	9
	MULTX	1E-06	36	36	49	60	1	14
	MULTY	3	36	78	1	48	1	14
A24	MULTX	0.2	40	55	23	56	1	37
	MULTX	1E-06	13	13	31	50	1	9
	MULTX	0.35	40	55	57	75	1	37
	MULTY	0.001	38	78	79	131	13	37
	MULTY	0.5	1	18	18	38	1	16
	MULTY	5	33	78	53	78	1	37
	MULTZ	0.001	37	78	13	40	16	16
	MULTZ	0.001	47	78	13	40	14	14
	MULTZ	10	38	78	79	131	13	37
	MULTZ	0.001	13	53	12	42	9	9
	MULTX	1E-06	36	36	49	60	1	14
	MULTY	2.5	36	78	1	48	1	14
A25	MULTX	0.2	40	55	23	56	1	37
	MULTX	1E-06	13	13	31	50	1	9
	MULTX	0.35	40	55	57	75	1	37
	MULTY	0.001	38	78	79	131	13	37
	MULTY	0.5	1	18	18	38	1	16
	MULTY	5	33	78	53	78	1	37
	MULTZ	0.001	37	78	13	40	16	16
	MULTZ	0.001	47	78	13	40	14	14
	MULTZ	10	38	78	79	131	13	37
	MULTZ	0.001	13	53	12	42	9	9
	MULTX	1E-06	36	36	49	60	1	14
	MULTY	2.2	36	78	1	48	1	14